ALMA MATER STUDIORUM · UNIVERSITÀ DI BOLOGNA

SCHOOL OF SCIENCE
Department of Physics and Astronomy
Master Degree Programme in Astrophysics and Cosmology

Statistical properties of young Brown Dwarfs and their disks in simulated Star formation environments

Graduation Thesis

Presented by:
Giovanni Mazzarini

Supervisor:
Leonardo Testi

Co-supervisor:
Ugo Lebreuilly
Alice Somigliana

Academic year 2023-24

Graduation date 27-03-2025

Contents

Abstract

The present work comprises a comparative study with a focus on the statistical properties of young stars and brown dwarves and their protoplanetary disks, as extracted from numerical simulations of stellar cluster formation. In order to examine how the inclusion of magnetic fields and radiative processes influences the formation and evolution of disks as well as the distribution of stellar masses, we compare the classical hydrodynamic SPH simulations by Bate with new magnetohydrodynamic (MHD) simulations. The latter include non-ideal effects such as ambipolar diffusion, radiative feedback, and, in some cases, sub-grid treatments for protostellar jets. A central objective of the study has been the exploration of extreme regions in the parameter space of protoplanetary disks, with particular emphasis on the correlations between disk mass, stellar mass, accretion rates, and radius distributions. Through a comparative analysis of results obtained with classical and MHD models, the thesis aims to assess the robustness of existing theoretical frameworks and to identify potential discrepancies arising from the introduction of additional physical ingredients, such as the influence of magnetic fields and feedback mechanisms. The results of the study demonstrate that, while Bate's model provides a robust framework for simulating disk and brown dwarf formation, the incorporation of magnetic and radiative effects results in substantial variations in disk properties, impacting both angular momentum transport and the fragmentation process of molecular clouds. We identify a variety of observables that could be compared with models to understand the importance of the different physical effects in different star formation environments. Our methodology can be expanded in the future to analyze a broader set of simulations covering the diversity of environments expected in the Galaxy. Ultimately, these methodology will allow us to define the initial conditions for planet formation.

Chapter 1

Theoretical Introduction

1.1 Star and Planet Formation and Evolution

1.1.1 The Birthplace: Molecular Clouds

Molecular clouds are defined as dense, cold regions of the interstellar medium (ISM) composed primarily of molecular hydrogen (H_2) and dust grains. It is important to note that these clouds are shielded from ultraviolet radiation, which is a prerequisite for the process of star formation. The low temperatures (approximately 10–20 K) present in these clouds allow gravitational collapse to proceed efficiently without being counteracted by thermal pressure [25]. The composition of molecular clouds is largely preserved by this shielding, which protects the gas from external radiation. Typically spanning tens to hundreds of parsecs, these clouds contain masses ranging from a few hundred to several million solar masses [44]. Giant molecular clouds (GMCs) are the most massive and well-studied examples. They function as stellar nurseries, providing a environment conducive to the formation of both low- and high-mass stars [20].

Molecular hydrogen is the most abundant molecule, but it is difficult to observe directly due to its lack of a permanent dipole moment. Consequently, astronomers have adopted carbon monoxide (CO) as a tracer, given its strong emission in the millimeter and submillimeter wavelengths [63]. Observations of CO have revealed the turbulent nature of these clouds, with supersonic motions playing a crucial role in shaping their structure and evolution. The incorporation of turbulence as an additional factor influencing cloud structure, in conjunction with magnetic fields, facilitates a more comprehensive understanding of the reshaping of gas structures in the ISM. This turbulence, in combination with gravitational forces and magnetic fields, determines the fragmentation of clouds into smaller, denser regions known as clumps and cores [39]. The process of star formation is not uniformly distributed across molecular clouds; instead, it occurs in concentrated dense regions such as clumps and filaments, which possess masses of $10^3 M_\odot$ and sizes ranging from 0.1 to 1 parsec.

These regions have the capacity to disintegrate into smaller scales and evolve into cores, where the process of star formation begins [55].

Recent studies have indicated that molecular clouds are not long-lived structures; rather, they are transient features of the ISM. These clouds form and disperse over timescales of 10–30 Myr as a result of stellar feedback, shear forces and large-scale galactic dynamics [18]. Comprehension of the lifecycle of these clouds is essential for the development of theories concerning star formation and galactic evolution. As the dense material within these clumps undergoes gravitational collapse, the initial rotational velocity increases, and the angular momentum becomes significant at smaller scales. This process gives rise to the formation of a disc-like configuration around the nascent protostar. The attainment of thermodynamic equilibrium by the protostar marks the onset of hydrogen burning in its core, thus leading to its evolution into a main-sequence star.

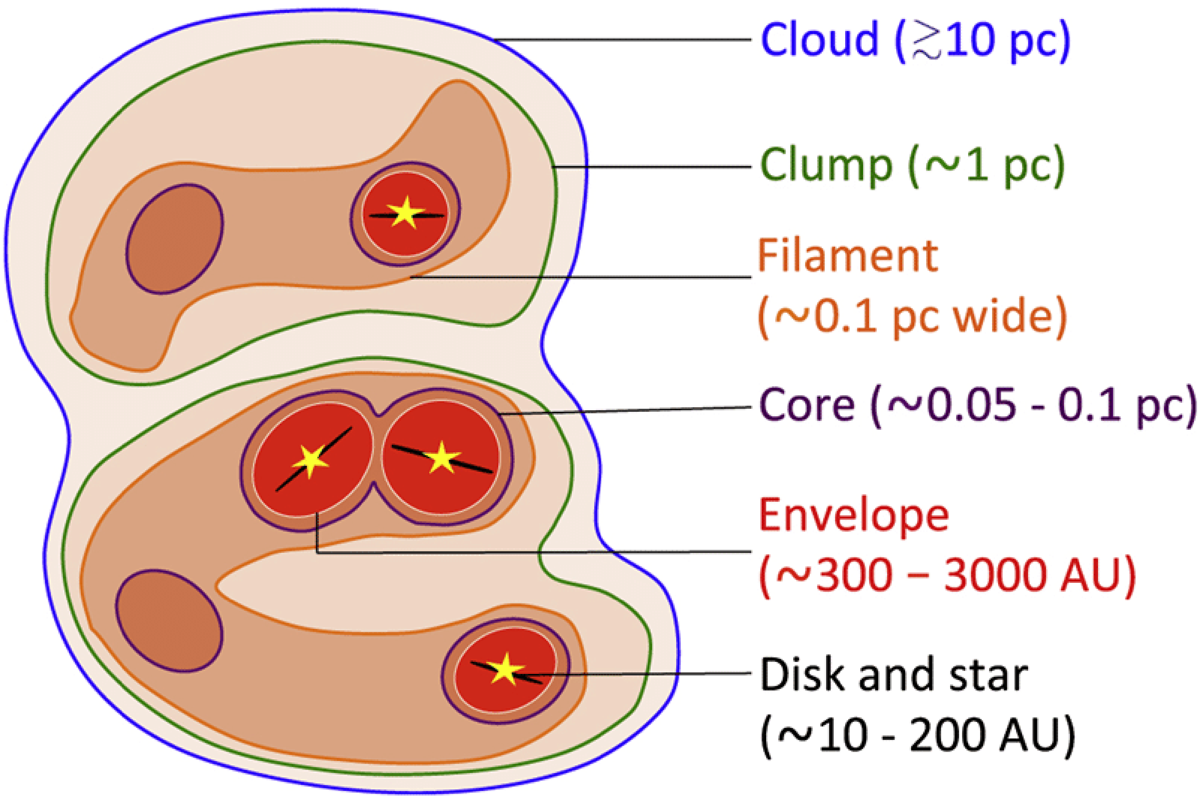

Figure 1.1: Molecular Clouds Hierarchical Structure.

1.1.2 The formation of protoplanetary disks

Conservation of angular momentum and disk formation

The primary physical interest of protoplanetary disks lies in their status as the precursors of planets. These disks provide the optimal environment for planet formation by supplying the material from which planetary cores grow. Additionally, they are responsible for supplying the gas necessary for the formation of planetary atmospheres. Protoplanetary discs originate during the star formation process and store the excess angular momentum.

If we consider the angular momentum of a point mass M_p orbiting the Sun, it is given by:

$$J_p = M_p \sqrt{G M_\odot a_p} \tag{1.1}$$

where a_p is the orbital semi-major axis. For Jupiter, this results in:

$$J_p = 2 \times 10^{50}\,\mathrm{cm}^2\,\mathrm{g}\,\mathrm{s}^{-1} \tag{1.2}$$

Instead of computing the angular momentum of the Sun explicitly, we can analyze the ratio between the angular momentum of Jupiter and the Sun:

$$\frac{J_p}{J_\odot} = \frac{M_p \sqrt{G M_\odot a_p}}{k M_\odot R_\odot^2 \Omega} \tag{1.3}$$

where k is a constant of order unity. Substituing the numerical values, we obtain:

$$\frac{J_p}{J_\odot} \approx \frac{2 \times 10^{50}}{3 \times 10^{49}} = \frac{20}{3} \tag{1.4}$$

which shows that the angular momentum of Jupiter alone is an order of magnitude larger than that of the Sun. Moreover, the total angular momentum of the Solar System is found to be several orders of magnitude lower than the initial angular momentum of molecular cloud cores, estimated to be around $10^{53}\,\mathrm{cm}^2\,\mathrm{g}\,\mathrm{s}^{-1}$. This finding suggests that a substantial portion of the initial angular momentum must have been transferred to other regions during the collapse process. The prevailing hypothesis suggests that this excess angular momentum is stored in rotationally supported structures, specifically protoplanetary disks. Nevertheless, the precise physical mechanisms responsible for angular momentum transport outward remain an open question. The advent of substantial data on exoplanets has enabled the acquisition of detailed information regarding their dynamics, composition, and the potential for life. Since the first detection of an exoplanet around a main sequence star [45], this field of research has grown exponentially. The majority of discovered planets differ significantly from those of our Solar System. These disparities imply that our Solar System may not be so typical after all.

This finding has had a profound impact on the field, leading to a paradigm shift in the theories that had previously been linked to the reproduction of the Solar System architecture. Contemporary theories propose that the formation of planets typically takes place over a timescale of a few million years, which is comparable to the duration of the protoplanetary disc. This profoundly links the disc evolution to the planet formation. A crucial element in this process is the nature and availability of the building blocks of planets, known as planetesimals. The chemical evolution of the disc, in conjunction with the physical driving mechanisms, contributes to the modification of the region conducive to planet formation. Recent high-resolution observations (e.g., ALMA) have revealed complex substructures such as rings and gaps, which are indicative of early planet formation [5].

YSO Classification

The classification of Young Stellar Objects (YSOs) is primarily based on the infrared excess in their spectral energy distribution (SED), which reflects the presence and evolution of circumstellar material [41]. The infrared spectral index is a key parameter used to classify YSOs, defined as:

$$\alpha_{IR} = \frac{d \log(\lambda F_\lambda)}{d \log \lambda} \tag{1.5}$$

where λ is the wavelength and F is the flux density at that wavelength. This index quantifies the slope of the SED in the infrared range, providing a measure of the excess emission due to circumstellar material. The classification is divided into four main stages, depending on the value of α_{IR}:

- **Class 0**: This initial phase of star formation is characterized by an embedded protostar within a dense envelope, making direct optical observation impossible. These objects are primarily detected via millimeter and submillimeter wavelengths. The infall of material occurs both directly from the envelope and through an accretion disk. The conservation of angular momentum results in the launching of powerful bipolar jets and molecular outflows, which help regulate angular momentum transfer [27].

- **Class I**: The protostar becomes more prominent as the envelope mass decreases due to accretion and outflow activity. Although still partially enshrouded by circumstellar material, these objects begin to exhibit infrared excesses characteristic of an emerging disk. The accretion process continues, accompanied by magnetically controlled jets and winds that further shape the surrounding environment [32] . Class I objects are identified by an infrared spectral index $\alpha_{IR} \geq 0.3$.

- **Class II**: Also known as protoplanetary disks, this phase corresponds to systems where most of the envelope has dissipated, leaving a well-defined circumstellar disk. The disk evolves under the effects of viscosity, turbulence, and magneto-hydrodynamic (MHD) winds, which facilitate angular momentum redistribution and accretion onto the central star [4]. Dust particles within the disk coagulate into larger aggregates, eventually forming planetesimals and planetary embryos [38]. Class II objects are characterized by an infrared spectral index in the range $-1.6 \leq \alpha_{IR} < -0.3$.

- **Class III**: The final stage before the main sequence, characterized by the near-complete dispersal of the circumstellar disk. Any residual material is either accreted onto the star, incorporated into planetary bodies, or expelled by stellar winds and radiation pressure. At this point, the young star becomes fully visible in optical wavelengths, and only a tenuous disk or debris disk remains, potentially giving rise to second-generation planet formation [23]. Class III objects exhibit little to no infrared excess and have $\alpha_{IR} < -1.6$.

The transition timescales between these phases vary, with Class 0 objects typically lasting 10^4 years, Class I around 10^5 years, and Class II and III spanning a few Myr [24]. The study of these stages provides crucial insights into the timeline of star and planet formation, linking the collapse of molecular clouds to the emergence of planetary systems.

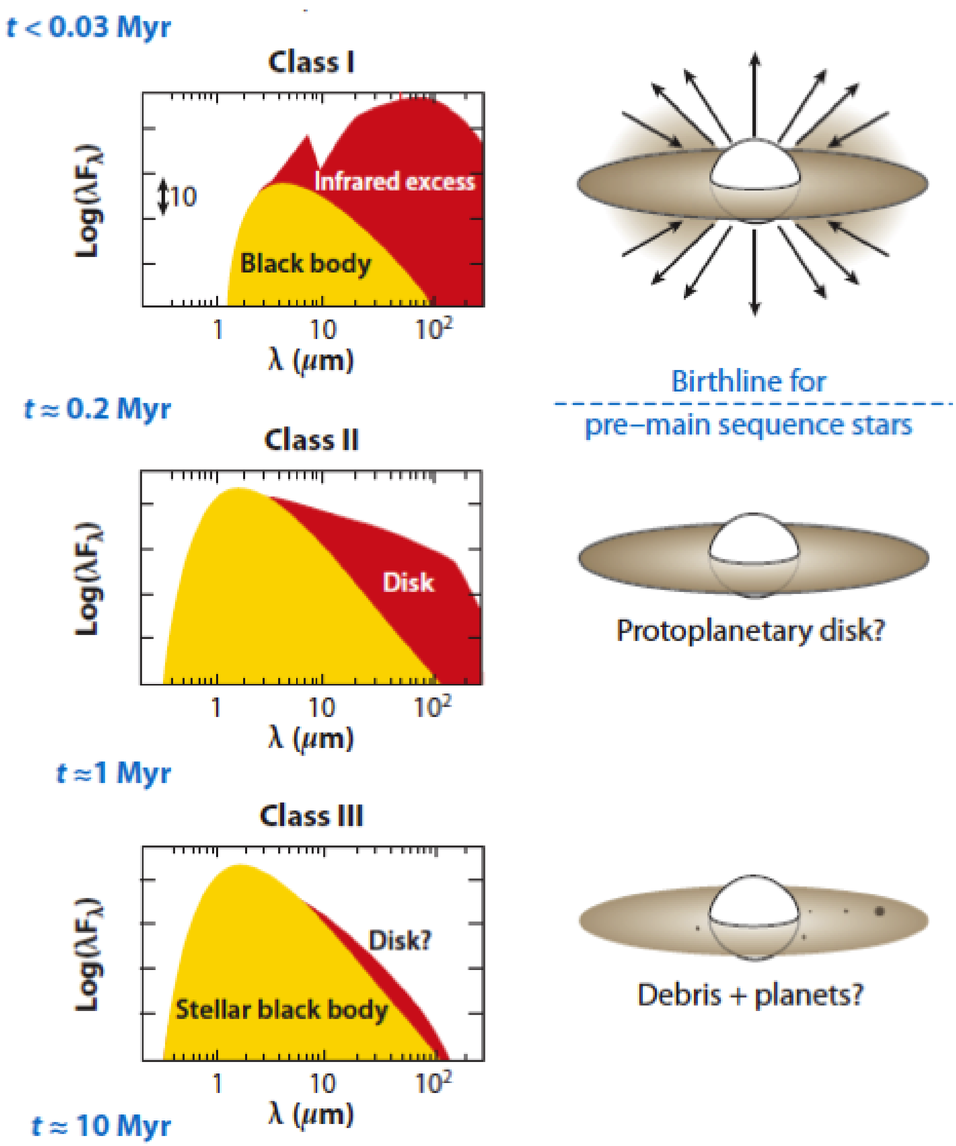

Figure 1.2: YSO classification scheme.

1.1.3 Brown dwarfs: characteristics and peculiarities of their discs

Brown dwarfs are substellar objects with masses below approximately 0.075 $M_{\odot}$, the threshold below which hydrogen nuclear fusion cannot be sustained in a stable manner. The theoretical conception of these objects can be traced back to the 1960s, when they were first theorised by Kumar [40] and Hayashi and Nakano [34]. They demonstrated that, for objects with masses below the aforementioned limit, the gravitational collapse of a molecular cloud is impeded when the thermal pressure increases, owing to the increasing opacity of the gas. This phenomenon can be understood as follows: during the process of collapse, when the density of the gas reaches levels that render it opaque to radiation, the cooling process is suppressed, thereby preventing further contraction of the fragment. This fragmentation limit due to opacity establishes a minimum mass – on the order of a few Jovian masses – which is naturally found in simulations and is the starting point for the formation of brown dwarfs. Such objects then continue to cool and contract over time, displaying very low luminosity and peculiar spectral characteristics. In the hydrodynamic simulations conducted by Bate [11], the fragmentation limit was resolved, and a mass distribution was produced that included numerous objects with masses equal to a few Jovian masses. This result is in line with the natural formation of brown dwarfs. The introduction of radiative feedback [12] has been demonstrated to influence the collapse of protostellar cores, thereby limiting excessive fragmentation and achieving a star-to-brown dwarf ratio that is more consistent with observations. Recent studies have demonstrated that, despite the fact that brown dwarfs are born through mechanisms analogous to those of higher-mass stars, the discs surrounding them are typically smaller and less massive [13]. These discs, however, have been shown to offer potentially suitable environments for the formation of planetary bodies. In summary, brown dwarfs are formed as an integral part of the star formation continuum. The discs surrounding them serve as natural laboratories for studying planetary formation in low-mass environments. They also allow exploration of the extreme conditions of the accretion and fragmentation process, thus expanding our understanding of the entire spectrum of planetary systems.

1.2 Properties and Evolution of Protoplanetary Disks

1.2.1 Mass and Composition (gas vs dust)

Protoplanetary disks are composed primarily of gas and dust. The mass of gas is approximately 99 % of the total mass of the disk, with the remaining 1% being made up of dust [36]. This composition is inherited from the interstellar medium, where the gas-to-dust mass ratio is typically around 100:1. The gas in protoplanetary disks is predominantly molecular hydrogen (H_2), accounting for approximately 74 % of the mass. The remaining 25% is helium, with the remaining 1% consisting of heavier elements. The observation of the gas component presents a significant challenge, as molecular hydrogen and helium do not radiate efficiently at typical temperatures of protostellar disks. Molecules with permanent dipole moment and dust grains are the most efficient at radating at low temperatures through rotational transitions and continuum emission respectively. Consequently, astronomers rely on alternative tracers, such as carbon monoxide (CO) and its isotopologues, to estimate gas masses. However, these methods are susceptible to factors such as CO depletion and uncertain conversion ratios, which can introduce variability and inaccuracy into the gas mass estimations [62].

Dust particles, despite constituting a negligible proportion of the disk's mass, play a pivotal role in the evolution of disks and the formation of planets. Furthermore, its emission at millimiter wavelengths is easier to detect than that of gas, and it can be utilised to calculate the total disk mass by employing the gas-to-dust ratio. The observed flux density, F_ν, is related to the dust mass by the following equation:

$$F_\nu = \frac{B_\nu(T_d)\bar{\kappa}}{d^2} M_{dust} \tag{1.6}$$

where B_ν is the Planck spectrum at the dust temperature and $\bar{\kappa}$ is the opacity . This equation provides a method to infer the dust mass from observational data.

Dust particles are initially sub-micron-sized grains composed of materials such as graphite and silicate minerals (e.g. olivine, pyroxene, forsterite) in both crystalline and amorphous forms [36]. As the disk evolves, dust grains can grow to millimetre sizes and beyond, leading to decoupling from the gas, settling towards the midplane, and concentrating in regions of higher pressure. This process is of paramount importance for the formation of planetesimals and, ultimately, planets. The gas-to-dust ratio in protoplanetary disks can evolve over time due to a variety of processes, including dust grain growth, settling, and radial drift. A comprehensive understanding of the mass and composition of these disks is imperative for investigating the initial conditions of planet formation and the subsequent diversity of planetary systems.

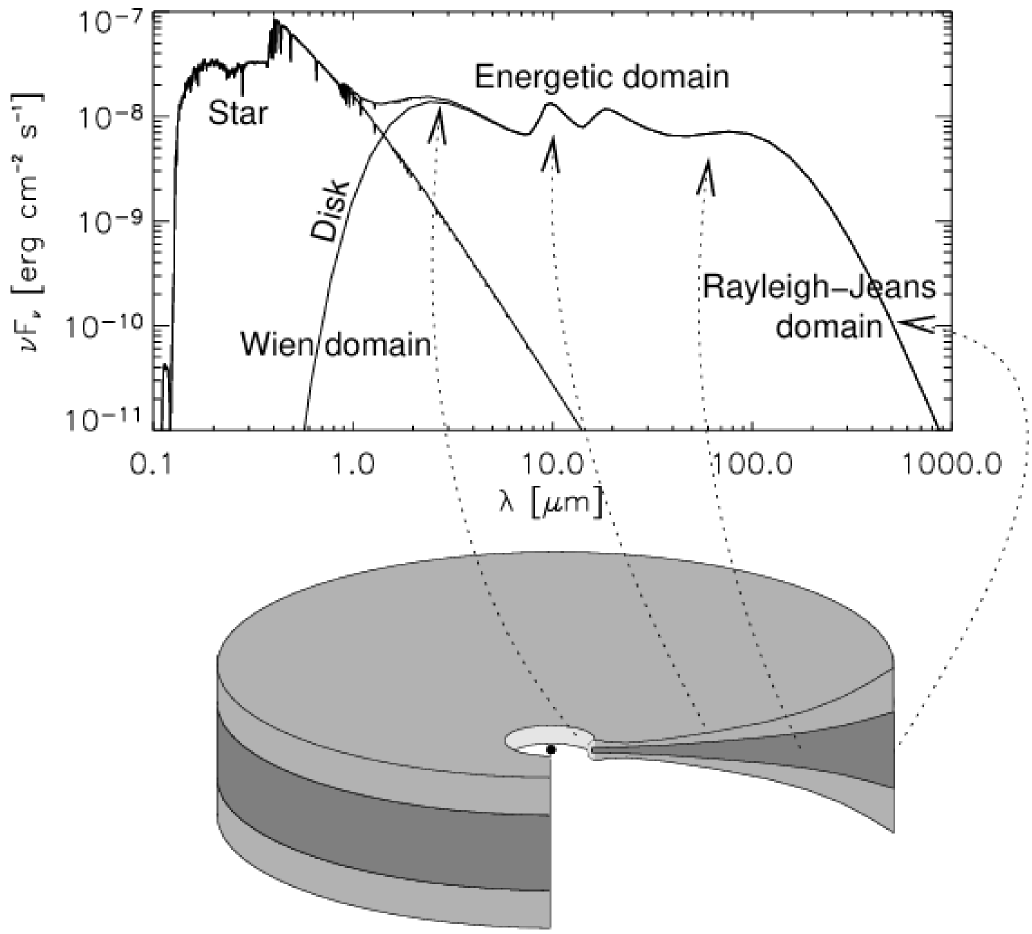

Figure 1.3: Contributions of the different regions of the disk to the overall spectral energy distribution.

Vertical Hydrostatic Equilibrium

The vertical structure of a protoplanetary disk is determined by the balance between the pressure gradient force and the vertical component of the star's gravitational force. This balance is described by the vertical hydrostatic equilibrium equation:

$$c_s{}^2 \frac{d\rho_g}{dz} = -\rho_g \frac{GM_*}{r^3} z = -\rho_g {\Omega_k}^2 z \tag{1.7}$$

where:

- c_s is the isothermal sound speed
- ρ_g is the gas density
- M_* is the mass of the central star
- r is the radial distance from the star
- z is the vertical height above the disk plane
- Ω_k is the Keplerian angular velocity

This equation demonstrates that the gas pressure declines with increasing height above the midplane, thereby counteracting the vertical gravitational force of the star. The solution to the equilibrium equation results in a Gaussian distribution of the gas density:

$$\rho_g = \rho_0 \exp(\frac{-z^2}{2{H_p}^2}) \tag{1.8}$$

where:

- ρ_0 is the midplane gas density
- H_p is the pressure scale height of the disk

This expression indicates that the density decreases exponentially with the square of the distance from the midplane, defining a thin, flared structure typical of protoplanetary disks.

Disc Radial structure

The radial structure of protoplanetary disks is characterised by systematic variations in surface density and temperature as a function of distance from the central star. These properties have important implications for accretion processes and disk dynamics. The surface density of the disk, denoted as $\Sigma(r)$, tends to decrease with radius following a power-law distribution:

$$\Sigma(r) = \Sigma_0(\frac{r}{r_o})^{-p} \tag{1.9}$$

where Σ_0 is the surface density at a reference radius r_0 and p is an index typically ranging between 0.5 and 1.5 [22]. Similarly, the temperature profile of the disk follows a power-law relation:

$$T(r) \propto r^{-q} \tag{1.10}$$

where q is generally between 0.5 and 0.75, depending on the dominant heating and cooling mechanisms in the disc. The temperature affects the scale height of the disk and the speed of sound, both of which are critical for gas dynamics and angular momentum transport. The influence of radial structures on accretion mechanisms within disks is a subject of significant interest in the field of astrophysics. For example viscosity, which governs angular momentum transport, is contingent on gas temperature, density and ionization. In regions exhibiting higher surface density and lower temperatures, accretion can be less efficient, whereas in areas of higher temperatures, viscosity increases, thereby facilitating angular momentum transport and material accretion onto the star. The radial structure of protoplanetary disks is a crucial aspect to be understood for the purpose of accurate modelling of planetary formation processes and the evolution of stellar systems.

1.2.2 Dynamics and Accretion Mechanisms

Protoplanetary discs are defined as rotating structures composed primarily of gas and dust, which envelop young stars. The dynamic evolution of these discs is determined by angular momentum transport processes, which facilitate the inward spiral of material towards the central star through accretion mechanisms. A comprehensive understanding of these processes is imperative to elucidate the formation of planets and the evolution of planetary systems. In order for the gas in the disc to accrete on the central star, it must first lose angular momentum. This process of transport is mediated by several physical mechanisms:

- **Turbulence Induced by Magneto-rotational Instability (MRI)**: in the presence of weak magnetic fields, magneto-rotational instability (MRI) has been shown to generate turbulence in the disc, thereby acting as an effective mechanism for transporting angular momentum. This turbulence has been demonstrated to increase the effective viscosity of the disc, thus facilitating the accretion of material towards the central star [8].

- **Hydrodynamic Instabilities**: in the absence of significant magnetic fields, purely hydrodynamic instabilities have been shown to induce turbulence and contribute to angular momentum transport [43]. However, the effectiveness of these mechanisms is still being studied.

- **Transport by spiral density waves**: density waves, generated by perturbations in the disc, have been shown to transport angular momentum, thereby causing a net transfer of mass towards the star. This mechanism is of particular relevance in discs exhibiting gravitational instabilities [53].

The viscous torque is a pivotal factor in the redistribution of angular momentum within the disc, and can be expressed as follows:

$$g(R) = -2\pi R^3 \nu \Sigma \frac{d\Omega}{dR} \tag{1.11}$$

where $\frac{d\Omega}{dR}$ represents the radial gradient of the angular velocity. The equation under consideration provides a quantitative framework for understanding how viscous forces act within the disc to transfer angular momentum outward, thereby enabling material to move inward towards the central star. The equation thus provides a quantitative framework for understanding how viscous processes regulate the structure and evolution of protoplanetary discs. The efficiency of angular momentum transport is frequently characterised in terms of the disc's effective viscosity. The characteristic timescale for viscous evolution, known as the viscous timescale, is given by:

$$t_{visc} = \frac{R^2}{\nu} \tag{1.12}$$

where ν is the kinematic viscosity of the disc. A widely used prescription for the kinematic viscosity in accretion discs is provided by the Shakura-Sunyaev model, where viscosity is parameterized as:

$$\nu = \alpha c_s H_p \tag{1.13}$$

where α is the dimensionless Shakura-Sunyaev parameter that characterizes the efficiency of angular momentum transport. The α parameter encapsulates the effects of turbulent processes within the disc, with typical values ranging from 10^{-4} to 10^{-2} for protoplanetary discs [37].

Finally, in the case of discs exhibiting gravitational instabilities, transport by spiral density waves is found to be fundamental in order to remove angular momentum. In order to quantify this process, the Toomre stability criterion may be used:

$$Q = \frac{c_s \Omega_k}{\pi G \Sigma} \tag{1.14}$$

Q is the Toomre parameter and when $Q < 1$ the disk is gravitationally unstable and can undergoes fragmentation, potentially leading to the formation of planetary bodies. This criterion helps to identify regions within the disc that are prone to such instabilities. However, as the critical value of Q approaches 1, density enhancements known as spiral arms are developed within the disk. These spiral arms heat up the gas, rearrange the surface density, and stabilise the disk. It is therefore evident that an additional condition is required for disk instability to result in the formation of planets. This can be achieved through the cooling mechanism of the disk, which serves to counteract the heating and shearing effects. However, the efficiency of this process remains a subject of ongoing debate [28]. Another critical aspect of the accretion process is the energy released as material falls onto the central star. This is known as the accretion luminosity:

$$L_{acc} = \frac{G M_* \dot{M}}{R_*}(1 - \frac{R_*}{R_m}) \tag{1.15}$$

where R_m is the magnetospheric truncation radius. This equation quantifies the energy output resulting from the gravitational potential energy released as matter accretes onto the star. It is important to note that this equation serves to highlight the efficiency of the accretion process, with the understanding that this efficiency is dependent on the stellar parameters and the structure of the magnetic field. Additionally, the mass accretion rate itself is often expressed through the relation:

$$\dot{M} = 3\pi\nu\Sigma \tag{1.16}$$

where Σ is the disk surface density. This equation establishes a correlation between the viscosity of the disc and the rate of mass transport inward, thereby providing insights into the evolution of protoplanetary discs and the temporal dynamics of planet formation.

The accretion process in protoplanetary discs is characterised by a series of distinct stages and mechanisms:

- **Accretion of Dust and Formation of Planetesimals**: Dust particles within the disc collide and aggregate, forming larger and larger structures, from pebbles to planetesimals. The dynamics of the gas and dust, incorporating processes such as radial drift and turbulence, exert a substantial influence on the efficiency of accretion and the size distribution of the particles [16].

- **Gas accretion**: Following the formation of planetary cores, the accretion of gas from the surrounding disc becomes possible, particularly if these cores attain sufficiently high masses. The rate of gas accretion is contingent on the viscosity of the disc, the availability of material, and the core's capacity to cool and contract.

- **Magneto-centrifugal Winds and Photoevaporation**: In addition to accretion, discs can lose mass through magnetocentrifugal winds and photoevaporation processes induced by stellar or external radiation. These mechanisms influence the structure of the disc and the rate of accretion onto the central star [33].

Recent studies utilising high-resolution observations, such as those obtained with ALMA, have enabled the probing of the three-dimensional structure of gas velocity in protoplanetary discs, thereby providing observational constraints on accretion mechanisms and the presence of young planets [52]. A comprehensive understanding of the dynamics and mechanisms of accretion in protoplanetary discs is imperative for the development of precise models of planetary formation and the evolution of stellar systems.

1.2.3 Winds and Disk Dissipation Processes

Protoplanetary discs are dynamic structures subject to various processes that determine their evolution and dissipation. Among these, disc winds play a crucial role in the removal of material and the regulation of stellar accretion. Disc winds are defined as gas streams that are ejected from the disc surface with a large angular aperture. This is in distinction to collimated jets, which are characterised by the ejection of gas at much higher velocities ($v > 100$ km/s). The observation of these winds is facilitated through the utilisation of forbidden emission lines, such as [Ne II] (12.81 μm) and [O I] (6300 Å). Recent observations made with the James Webb Space Telescope (JWST) have enabled the acquisition of hitherto unpublished details concerning the gas flows within protoplanetary discs. These flows exhibit significant variations in both speed and direction, thereby influencing the distribution of material within the disc and, consequently, the formation of planets [3].

With regard to the dissipation of the disc, this process occurs principally via two mechanisms:

- **Photoevaporation**: The star's ultraviolet and X-ray radiation has been observed to ionise and heat the gas, thereby enabling it to reach speeds sufficient to escape the disc's gravitaty. This process is purely thermal and does not result in a significant loss of angular momentum. They are driven by stellar radiation and mainly remove gas from the outer regions of the disc. This process becomes dominant in the final stages of the disc's life and contributes to its disruption on timescales of a few million years [30]. In order to investigate this process, the gravitational radius can be utilised in order to ascertain the critical radius at which the gas becomes unbound from the star:

$$R_g = \frac{GM_*}{{c_s}^2} \tag{1.17}$$

  This formula delineates the radius at which the thermal energy of the gas is equivalent to the gravitational binding energy. Beyond this radius, the gas may escape, thereby significantly influencing the mass-loss rate and the overall evolution of the disk.

- **Magneto-hydrodynamic winds**: These winds are launched from different regions of the disc and can reach higher speeds. Unlike photoevaporative winds, MHD winds can remove angular momentum and influence the transport of material in the disc. They are driven by magnetic forces, with a resultant effect of the removal of gas and angular momentum from various locations on the disc. The efficiency of angular momentum extraction by MHD winds can be characterized by a dimensionless parameter, λ , defined as

$$\lambda = \frac{L}{R\Omega(R)} \tag{1.18}$$

  where L is the specific angular momentum in the wind, λ is the ratio of the extracted to Keplerian specific angular momentum [15]. A higher value of λ indicates more efficient angular momentum removal, which facilitates mass accretion onto the star. MHD winds are believed to be particularly significant in the inner regions of the disk, where magnetic field strengths are higher.

Recent studies suggest that MHD winds may be a dominant mechanism in disc dissipation, especially in the early stages of disc evolution [7]. A comprehensive understanding of these processes is essential for determining the timing and conditions of planetary formation, as well as for interpreting observations of protoplanetary discs at different evolutionary stages.

1.3 Observations and Theoretical models

1.3.1 Observational techniques and recent findings

The study of protoplanetary disks and protostars has been hugely aided by advances in observational techniques, particularly in the infrared and millimetre range, which have made it possible to obtain high-resolution images and details that are fundamental to understanding star and planet formation processes. Infrared observations are crucial for studying regions obscured by dust at visible wavelengths. Instruments such as the Hubble Space Telescope (HST) have revealed the presence of protoplanetary disks around protostars, known as 'proplyds', in star-forming regions such as the Orion Nebula. These observations have shown that the condensation of material is not spherical, but rather flattened due to the rotation of the progenitor cloud [1]. With the advent of the James Webb Space Telescope (JWST), infrared observing capabilities have been further enhanced. For example, JWST observed the star-forming region NGC 346 in the Small Magellanic Cloud and detected protoplanetary disks around low-metallicity stars. These observations suggest that planet formation may have been more common in the early universe than previously thought [21]. On the other hand, millimetre-scale observations with instruments such as the Atacama Large Millimeter/submillimeter Array (ALMA) have allowed the distribution of gas and dust in protoplanetary disks to be studied in unprecedented detail. ALMA has detected structures such as rings, spirals and gaps in the disks, which could indicate the presence of planets in the process of formation. These observations provide crucial constraints for theoretical models of planet formation. Instruments such as SPHERE (Short-Palmer High-Contrast Imaging Exoplanet Research) on the Very Large Telescope (VLT) have provided high-resolution images of protoplanetary discs, revealing a variety of complex morphological structures. For example, SPHERE has observed discs with concentric rings, spirals and shadows, suggesting dynamic interactions between the disc and possible planets in formation . These observations are key to understanding the physical processes that shape discs during the initial stages of planetary formation [29]. High-resolution spectroscopy represents a pivotal technique in the study of protoplanetary discs and protostars. Through the analysis of the spectral lines emitted by the gas in the disc, the chemical composition, temperature and dynamics of the gas can be determined. For instance, the observation of carbon monoxide (CO) emission lines facilitates the delineation of the gas distribution and the subsequent estimation of the disc mass.

Furthermore, mid-infrared spectroscopy facilitates the detection of complex molecules, providing insights into the prebiotic chemistry that occurs within these discs. Recent observations have led to significant discoveries, including:

- **Detection of Planets in Formation**: The integration of high-resolution imaging and spectroscopy facilitated the identification of candidate planets forming within the discs, thereby providing direct evidence of planetary accretion processes.

- **Complex Structures in Discs**: A variety of structures have been observed in the discs, including rings, spirals and gaps. These are interpreted as evidence of interactions between the disc and planets that are obscured within it.

- **Complex organic molecules**: The presence of complex organic molecules in the discs indicates that the fundamental components of life may have been formed during the earliest phases of planetary system formation.

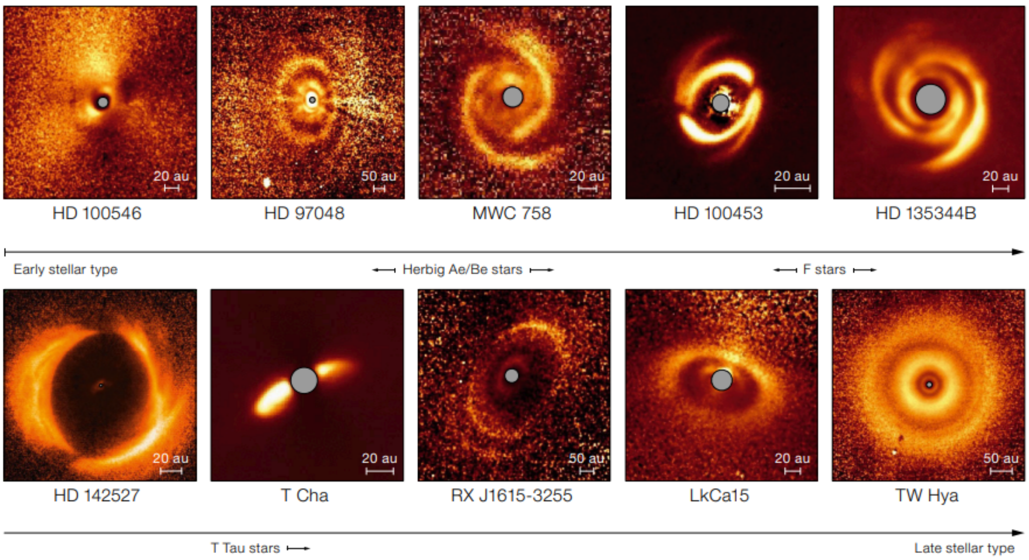

Figure 1.4: Collection of images of protoplanetary discs observed in PDI (Polarimetric Differential Imaging) with SPHERE.

1.3.2 Challenges in modeling disks and planet formation

The processes governing planet formation within protoplanetary disks represent a significant challenge in modern astrophysics. Despite considerable advances in both observational and theoretical research, many fundamental aspects remain poorly understood, particularly concerning the early stages of disk formation and the initial conditions that set the stage for their evolution. In this thesis, we concentrate on these initial phases of disk assembly and investigate how different physical processes shape the birth environment of protoplanetary disks. It is acknowledged that observational data on these early phases is limited, and theoretical models are still being refined to capture the complex interplay of mechanisms that define disk properties at formation.

The measurement of the disc's mass

A significant challenge in this field pertains to the precise measurement of the mass of protoplanetary discs. Conventional estimations are predicated on the analysis of dust emission or rare isotopologues; nevertheless, these methodologies can yield indirect and occasionally erroneous outcomes. Recent studies have utilised gas velocity to obtain more direct measurements, thereby revealing that some observed structures, such as internal gaps in the discs, still have no clear explanation [51]

Discs Temporal Evolution

Current models suggest that protoplanetary disks dissipate within a few million years. However, recent observations with the James Webb Space Telescope (JWST) have indicated that, in the early universe, these disks could persist for longer periods, up to 20-30 million years. This finding necessitates a re-evaluation of existing disc evolution models to incorporate the possibility of protoplanetary disks persisting in low-metallicity environments [21].

Formation of planetesimals

The transition from dust particles to planetesimals represents a crucial, albeit as yet poorly understood, step in the process of planetary formation. The 'pebble drift' theory proposes that small icy fragments migrate from the outer to inner regions of the disc, releasing water vapour beyond the 'snow line'. The validity of this theory has been substantiated by recent observations made using the JWST, which have confirmed the presence of the aforementioned vapour. Nevertheless, further research is required to ascertain the impact of these processes on the final distribution of planetesimals and the composition of the resulting planets [2].

Influence of Magnetic Fields

Magnetic fields have been demonstrated to exert a pivotal influence on the dynamics of protoplanetary discs, impacting processes such as angular transport and jet formation. Magnetohydrodynamic (MHD) modelling has demonstrated that variations in magnetic field strength can substantially modify the properties of discs, including their mass and size. Nevertheless, the incorporation of magnetic effects in models remains a complex undertaking and necessitates further investigation [42].

Discs Asymmetrical Structures

High-resolution observations have revealed asymmetrical structures in the discs, including spiral arms and dust clusters. The formation of these structures may be attributed to interaction with hidden planets or intrinsic instabilities in the disc. The accurate modelling of these features necessitates a comprehensive understanding of disc dynamics and disc-planet interactions [54].

1.4 Open questions

The study of protoplanetary disks and planet formation has advanced significantly in recent years; nevertheless, several fundamental questions remain unresolved. A comprehensive understanding of these unresolved issues is imperative for the refinement of theoretical models and the interpretation of observational data. This section delineates the salient challenges pertaining to the core collapse framework and the temporal sequence of planet formation.

1.4.1 Missing Physical Ingredients in the Core Collapse Framework

The core collapse framework is a theoretical model that describes the gravitational contraction of dense molecular cloud cores, leading to the formation of stars and disks. Despite its foundational role, several physical processes are not yet fully understood:

- **Magnetic Field Interactions**: The role of magnetic fields during the collapse phase remains the subject of debate. Whilst magnetic braking is widely considered to regulate angular momentum, observations indicate that disks can form even under strong magnetic influence, thus suggesting a lack of consideration for key physical processes in current models [19].

- **Non-Ideal Magnetohydrodynamics (MHD) Effects**: It is crucial to understand processes such as ambipolar diffusion, Hall effect and ohmic dissipation, which are critical for comprehending disk formation. Nevertheless, the precise influence of these processes on angular momentum transport and disk stability remains to be fully elucidated [60].

- **Turbulence and Fragmentation**: The mutual interaction between turbulence within molecular clouds and fragmentation during collapse exerts a significant influence on the initial mass function of stars and the formation of binary or multiple systems. The quantification of the scale and impact of turbulence remains an ongoing challenge [50].

- **Feedback Mechanisms**: Stellar feedback, including jets, outflows, and radiation pressure, influences the collapse process and subsequent disk evolution. The efficiency and role of these feedback mechanisms in different environments remain unclear [27].

1.4.2 The Timeline of Planet Formation

Recent observations have reshaped our understanding of planet formation timelines. Dust masses in Class II protoplanetary disks appear insufficient to form the planetary systems we observe, suggesting that planet formation begins earlier, during the Class 0/I stages. Evidence from ALMA and VLA observations of young disks supports this early onset, highlighting the importance of studying embedded disks to unravel the processes of planet formation in its infancy. Determining the timescale of planet formation is of paramount importance for a comprehensive understanding of the diversity of planetary systems.The following key uncertainties must be given due consideration:

- **Rapid Disk Evolution**: Observations indicate that protoplanetary disks dissipate within 5-10 million years, yet giant planets appear to form within this short timescale. The mechanisms enabling such rapid growth, especially for gas giants, require further investigation [31].
- **Early Onset of Planet Formation**: High-resolution imaging techniques, such as ALMA, have revealed disk substructures indicative of planet formation in disks with a formation age less than 1 million years. This finding challenges the conventional models that assume the initiation of planet formation occurs subsequent to disk settling [5].
- **Pebble Accretion Efficiency**: The pebble accretion model provides a rapid pathway for core growth; however, its efficiency is contingent upon disk conditions that remain to be fully characterised. It is critical to understand the interplay between pebble flux, disk turbulence, and migration [49].
- **Late-Stage Planetary Dynamics**: The final architecture of planetary systems is shaped by dynamical interactions long after the gas disk dissipates. The modelling of these processes, including planet-planet scattering and migration, remains complex due to the chaotic nature of these interactions [17].

1.4.3 Additional Considerations

In consideration of the interconnected nature of disk evolution and planet formation, the following research questions require further investigation:

- **Chemical Evolution of Discs**: How does the chemical composition of disks evolve, and how does this influence planet composition and habitability potential? [48]
- **Impact of Stellar Environment**: the impact of external radiation fields and stellar encounters on disk longevity and planet formation efficiency in a range of star-forming environments [64].

- **Observational Limitations**: Theoretical models of disc and planet formation describe complex processes such as gas accretion, planetary migration and chemical evolution. However, the verification of these models requires direct observations, which are difficult to obtain due to technological limitations and the hidden nature of many processes within discs [56].

1.5 Thesis Objectives

The central aim of this thesis is to examine the manner in which magnetic fields, radiative feedback, and associated processes affect the formation and characteristics of protoplanetary disks and brown dwarfs. This investigation will be undertaken by comparing the findings of this study with those of classical Bate simulations. A particular emphasis will be placed on identifying how the inclusion of magnetic effects alters fragmentation, disk mass, and angular momentum transport, ultimately shaping the stellar mass distribution and the evolution of protostellar systems. The analysis is principally concerned with the following aspects:

- The relation between disc mass and stellar mass;
- Stellar accretion rate
- The cumulative fraction of stars produced
- The temporal evolution of key parameters related to the disc
- The correlations between the different disc parameters
- The distribution of masses and radii of the brown dwarfs selected from the simulation.

Additionally, the thesis explores an especially relevant parameter space for low-mass regimes, which are crucial for understanding brown dwarf formation, and examines the initial conditions that set the stage for planet formation.Through a comprehensive analysis of cumulative mass distributions, accretion rates, disk radii, and surface density, the aim is to elucidate the role of key parameters (such as Beta) in driving or suppressing fragmentation. By integrating theoretical models and observational constraints, this work identifies open questions and future research directions, ranging from longer-wavelength simulations and more accurate magnetic field measurements to the implementation of tracer particles. These directions are intended to advance our knowledge of star and disk formation in both typical and low-mass environments. A comprehensive examination of the models and data will be presented in Chapter 2.

Chapter 2

Comparative analysis of simulation models

2.1 Numerical simulations of protoplanetary systems

Numerical simulations have become an essential tool in astrophysical research, enabling the exploration of complex systems that are difficult or impossible to model analytically. By applying well-established physical laws through mathematical equations and solving them computationally, simulations allow researchers to study interactions among various processes in star-forming environments. This approach provides insights into the kinematics and dynamics of these systems. This chapter will present and compare two types of models that are used to study the formation of protoplanetary disks and brown dwarfs. Firstly, the classical Bate model will be presented, which has been a fundamental reference for the simulation of star formation using Smoothed Particle Hydrodynamics (SPH) techniques with the use of sink particles and, in some cases, the inclusion of radiative feedback. On the other hand, the new models replicate these processes, but also incorporate the influence of the magnetic field and mechanical feedback.

2.2 Previous Numerical Simulations

Bate's classical model has been a fundamental reference point for the numerical study of star formation, particularly with regard to the formation of protoplanetary disks and brown dwarfs. This model was developed using a code based on Smoothed Particle Hydrodynamics (SPH), the initial implementation of which dates back to the work of Benz [14] and was further modified by Bate and collaborators.

2.2.1 SPH methodology and dynamic adaptation

The Smoothed Particle Hydrodynamics (SPH) method is a computational technique that utilises a discrete, or cellular, approach to simulate the behaviour of fluids. In this approach, the fluid is represented by a set of particles, each of which possesses specific physical properties, including mass, density, velocity, and internal energy. A physical field $A(r)$ at a position r is approximated by a weighted sum over contributions from neighboring particles using a kernel function $W(r - r_j, h)$:

$$A(r) \approx \sum_j \frac{m_j}{\rho_j} A_j W(|r - r_j|, h) \tag{2.1}$$

where m_j and ρ_j are are the mass and density of particle j, respectively, and h is the smoothing length that defines the region over which the kernel is non-zero. A pivotal element of SPH is the dynamic adaptation of the smoothing length. In practice, the smoothing length is adjusted so that each particle interacts with a fixed number of neighbouring particles (typically around 50). This dynamic adaptation ensures higher resolution in high-density regions, since the smoothing length decreases as density increases. This allows for accurate resolution of processes such as gravitational collapse, fragmentation, and disk formation. This technique is essential to properly resolve the Jeans mass, thereby avoiding artificial fragmentation [59]. This approach was initially described and applied by Benz in his review of SPH techniques, and was subsequently developed further by Monaghan [46] and by Bate, Bonnell and Price [10]. The latter work introduced the concept of sink particles, whereby high-density regions, where the gas becomes optically thick and cooling is inefficient, are replaced by sink particles representing protostars or brown dwarfs. These sink particles continue to accrete material if the surrounding gas is gravitationally bound and possesses sufficiently low angular momentum.Combined with the dynamic adaptation of the smoothing length, this method enables high-resolution simulations of complex processes like gravitational collapse and the formation of multiple systems.

2.2.2 Calculation of Gravitational Forces

In Bate's models, gravitational interactions play a critical role in the processes of cloud collapse and subsequent star and brown dwarf formation, as well as disk formation. In order to compute these forces efficiently, the simulation employs a tree-based algorithm, a common technique in large-scale SPH simulations. Instead of calculating the gravitational force between every pair of particles directly – which would scale as N^2 – a hierarchical tree structure is constructed (typically a binary or Barnes-Hut tree). This algorithm groups distant particles together and approximates their collective gravitational effect by a multipole expansion, usually truncated at the monopole level (and in some cases including quadrupole corrections). Subsequently, an opening angle criterion is applied: if a group of particles is sufficiently distant from the particle under consideration, the group is treated as a single mass located at its centre of mass. This approach significantly reduces the number of force calculations required, typically scaling as $NlogN$ [9].

In high-density regions, particularly when particles come very close to each other, the gravitational force can become singular, which can result in numerical divergences. To avoid such issues, Bate's code employs gravitational softening, whereby a softening length is introduced so that for separations smaller than this length, the force is "smoothed" over a finite volume. This ensures that gravitational interactions remain finite and that dynamics on very small scales (below the resolution limit) are handled in a physically reasonable way.In simulations involving sink particles, gravitational interactions between sink particles, as well as between sinks and gas particles, are computed using this softened potential.

2.2.3 Sink Particles

In Bate's SPH simulations, the implementation of sink particles is imperative for the management of extreme densities encountered during gravitational collapse.As regions within a molecular cloud collapse, the gas density can exceed a critical threshold, which is often associated with the opacity limit for fragmentation. Beyond this threshold, the local Jeans mass increases and the required time steps become prohibitively short. To circumvent this problem, the simulation replaces these high-density, pressure-supported fragments with sink particles, which act as proxies for the newly formed protostars or brown dwarfs. The introduction of sink particles occurs when the density in a collapsing region reaches a predefined threshold. This ensures that the simulation does not need to resolve the internal dynamics of the fragment beyond that point.Once formed, a sink particle continues to accrete material from its surrounding environment. However, only gas that is within the specified accretion radius, gravitationally bound to the sink, and possessing sufficiently low angular momentum (such that it cannot form a stable orbit around the sink) is accreted. This accretion process enables the sink particle to accumulate mass over time, thereby circumventing the necessity to simulate the intricate microphysics of the fragment's core. The use of sink particles, originally described in Bate, Bonnell and Price [10], offers several advantages, as it prevents the simulation from stalling due to extremely small time steps required for dense regions, thereby enabling the study of the system's evolution over longer timescales. Moreover it facilitates the examination of multiplicity and disk formation, as sink particles interact gravitationally with each other and the surrounding gas, allowing the formation and evolution of circumstellar disks and multiple systems to be tracked. Nevertheless, the technique is not without its limitations. The selection of the sink accretion radius and the gravitational softening parameters has the capacity to exert influence on the small-scale dynamics, including the properties of close binary systems and the inner regions of circumstellar disks. This approach has been pivotal in enabling high-resolution simulations of star and disk formation, providing a robust framework to study the evolution of protostellar systems without being encumbered by the extreme physical conditions in the densest regions.

2.2.4 Radiative Feedback

In Bate's simulations, radiative feedback is found to be of crucial importance in regulating gravitational collapse and fragmentation in molecular clouds. This feedback is defined as the energy released by the formation of protostars, originating from both their intrinsic luminosity and the accretion process, and the subsequent impact on the surrounding gas. As a protostar is forming, its radiation heats the nearby gas, increasing the local thermal pressure and raising the Jeans mass. This heating acts to inhibit the further fragmentation of the gas, thereby reducing the number of very low-mass objects (e.g. brown dwarfs) that would otherwise form in a purely isothermal collapse. In previous simulations, a barotropic equation of state was employed, which posited that the gas remained isothermal up to a certain critical density before stiffening. However, these models failed to account for the additional heating provided by protostellar radiation. In his subsequent works, Bate incorporated radiative transfer using the flux-limited diffusion (FLD) approximation. In this framework, the radiative flux is computed as being proportional to the gradient of the radiative energy density. A flux limiter is employed to ensure that the flux does not exceed the free-streaming limit in optically thin regions. This approach enables the simulation to dynamically couple radiative heating and cooling to the gas energy equation, thereby yielding a more realistic temperature structure. Incorporating radiative feedback into Bate's models represents a significant advance over simpler barotropic approaches, yielding results that better reflect the complex interplay between radiation and hydrodynamics during star formation.

2.2.5 Resolution and Disk Studies

Bate's simulations achieve a high level of resolution, which is crucial for the study of the formation and evolution of protostellar disks.The code utilises the SPH method combined with the sink particle technique, enabling the resolution of disk structures on scales as small as approximately 10 AU [13]. This resolution is maintained by dynamically adjusting the smoothing length so that each particle interacts with a fixed number of neighbours, ensuring that even regions of very high density are adequately modelled. This meticulous approach is paramount to resolve the local Jeans mass at all times and to circumvent the occurrence of artificial fragmentation [59]. In practical terms, the simulations capture not only the global evolution of the protostellar disks, but also their internal properties, such as the radial surface density profiles, temperature gradients, and angular momentum distribution. For instance, by tracking the evolution of these disks over time, Bate's models provide robust statistical samples that enable comparisons with observational data (e.g. from ALMA). This level of detail allows researchers to analyse how the disk mass correlates with the central protostar's mass, how dynamical interactions truncate the disks, and how processes like accretion and radiative feedback shape their evolution. Furthermore, the utilisation of sink particles with meticulously calibrated accretion radii (ranging from approximately 5 AU in the original simulations to as low as 0.5 AU in re-run models) guarantees the proper resolution of the innermost regions of the disks, where a significant proportion of the angular momentum transport occurs. This is of particular significance when investigating the formation of close binaries and multiple systems, where disk interactions can exert a substantial influence on the outcome.

2.3 New ECOGAL RAMSES Models

Recent advancements in simulation techniques have permitted the extension of classical hydrodynamical models by incorporating non-ideal magnetohydrodynamics (MHD) effects. In the models under consideration, the full set of MHD equations – including ambipolar diffusion – is solved, and these are coupled with radiative transfer using the flux-limited diffusion (FLD) approximation. Sub-grid modelling of protostellar outflows is also employed. This framework is implemented in the RAMSES code [58] , which employs Adaptive Mesh Refinement (AMR) to resolve disk scales down to approximately 1–2 AU.

2.3.1 Initial Magnetic Field and Mass-to-Flux Ratio

The initialisation of the magnetic field is determined by the mass-to-flux ratio, μ, which is defined as follows:

$$\mu = \frac{\frac{M_0}{\Phi}}{(M_\Phi)_c} \tag{2.2}$$

where M_0 is the mass of the clump, Φ is the magnetic flux threading the clump, and $(M_\Phi)_c$ is the critical mass-to-flux ratio [47] given by

$$(M_\Phi)_c = \frac{0.53}{\pi}\sqrt{\frac{5}{G}} \tag{2.3}$$

This critical ratio delineates the threshold below which magnetic fields are capable of supporting the cloud against gravitational collapse. In practice, if $\mu > 1$, the cloud is considered to be magnetically supercritical (gravity dominates), while $\mu \leq 1$ indicates a subcritical cloud, i.e. one in which the magnetic field provides sufficient support against gravitational collapse. Observational studies (e.g., Crutcher 2012) have typically found that molecular clouds have dimensionless mass-to-flux ratios in the range of $\mu \approx 2 - 3$ [19], though values can vary depending on the environment. In the present study, an initial value of $\mu = 10$ is adopted in order to explore a regime where the magnetic field is relatively weak compared to gravity. This higher value tends to favour fragmentation and influences the angular momentum transport during collapse and disk formation. The magnetic flux, denoted by the symbol Φ, is calculated by integrating the magnetic field, denoted by the symbol B, over the area perpendicular to the field lines. It is evident that, in consideration of the initial conditions, the parameter μ is a pivotal factor in determining the initial magnetic field strength. For instance, in our models with a clump mass of $500 M_\odot$ and a radius of approximately 0.38 pc, $\mu = 10$ corresponds to an initial field strength of roughly $9,4 \times 10^{-5}$G. This parameter is of crucial significance as it influences the collapse dynamics of the clump, as well as the formation and evolution of circumstellar disks. A lower (or near-critical) mass-to-flux ratio would result in stronger magnetic support and possibly less fragmentation, while a higher value—as used here—allows for the study of disk formation and star formation in an environment where gravity is more dominant, but still influenced by magnetic effects.

2.3.2 Inclusion of Ambipolar Diffusion

In order to account for non-ideal MHD effects, the models under consideration incorporate ambipolar diffusion. In the context of magnetized star formation, the gas is found to be only partially ionized. Consequently, while the ions remain firmly coupled to the magnetic field lines, the neutral gas is capable of drifting relative to them – a process referred to as ambipolar diffusion. This decoupling is of paramount importance in dense molecular cloud cores, where the ionization fraction is found to be minimal. The process of ambipolar diffusion enables the collapse of neutrals under the influence of gravity, despite the presence of substantial magnetic support. This, in turn, has a significant impact on the fragmentation process and the subsequent evolution of protostellar disks. In the context of the MHD equations, ambipolar diffusion introduces an additional diffusion term in the induction equation. The modified induction equation can be written as:

$$\frac{\partial B}{\partial t} = \nabla \times (v \times B) - \nabla \times [\eta_{AD} \frac{|B|^2}{(\nabla \times B) \times B}] \tag{2.4}$$

The ambipolar diffusion coefficient, η_{AD} is typically given by

$$\eta_{AD} \approx \frac{B^2}{\gamma \rho_i \rho_n} \tag{2.5}$$

where ρ_i and ρ_n are the ion and neutral densities, and γ is the ion-neutral drag coefficient. In practice, the value of η_{AD} is derived through the utilisation of precomputed tables, as a function of the local gas density and temperature [35]. The incorporation of ambipolar diffusion within the simulation framework enables the gradual decoupling of the neutral component from the magnetic field. This effect is critical because:

- It facilitates gravitational collapse in regions where a strong magnetic field might otherwise halt or delay the process.
- It influences angular momentum transport, as the decoupling reduces magnetic braking in the densest regions, potentially affecting the size and structure of the resulting circumstellar disks.
- It modifies the fragmentation behavior within the collapsing clump, thereby impacting the mass distribution of protostars and brown dwarfs.

The incorporation of ambipolar diffusion within the new models provides a more realistic description of magnetised star-forming environments, particularly in the dense, poorly ionised regions where the majority of fragmentation and disk formation occurs.

2.3.3 Radiative Transfer Modeling

In the new models under consideration, radiative transfer is treated using the Flux-Limited Diffusion (FLD) approximation. This method effectively bridges the gap between the optically thick and thin regimes. In this approach, the radiative flux is expressed as:

$$F_r = -\frac{c\lambda}{\kappa_R \rho} \nabla E_r \tag{2.6}$$

where E_r is the radiative energy density, κ_R is the Rosseland mean opacity and λ is the flux limiter. The flux limiter is a function of the dimensionless parameter:

$$R = \frac{|\nabla E_r|}{\kappa_R \rho E_r} \tag{2.7}$$

and it ensures that in optically thin regions the flux does not exceed the free-streaming limit. The evolution of the radiative energy density is governed by the equation:

$$\frac{\partial E_r}{\partial t} + \nabla \cdot (vE_r) = -P_r \nabla \cdot v + \nabla \cdot (\frac{c\lambda}{\kappa_R \rho} \nabla E_r) + \kappa_P \rho c (a_R T^4 - E_r) \tag{2.8}$$

where P_r is the radiative pressure, κ_P is the Planck mean opacity and a_R is the radiation constant. The equation, which couples the radiation field to the gas dynamics, is solved using an implicit solver within the RAMSES code [58]. The implicit treatment is critical to handle the stiff coupling between the gas and radiation, particularly in dense regions where the cooling times are very short. In the present simulations, the gas and dust temperatures are assumed to be equal, a valid approximation in the high-density environments typical of protostellar disks. It is imperative to incorporate radiative transfer in order to accurately capture the protostellar feedback. As material accretes onto protostars, the resulting accretion luminosity:

$$L_{acc} = f_{acc} \frac{G M_{sink} \dot{M_{sink}}}{R_\star} \tag{2.9}$$

heats the surrounding gas. This heating has been shown to increase the local thermal pressure, thereby increasing the Jeans mass and, consequently, reducing the propensity for further fragmentation. This, in turn, results in a more realistic stellar initial mass function (IMF).By employing a precise modelling of the radiative transport of energy, these simulations are capable of determining the temperature structure within protostellar disks. This, in turn, exerts an influence on both the disk evolution and the conditions for planet formation.

2.3.4 Adaptive Mesh Refinement and Disk Resolution

In order to accurately capture the complex dynamics involved in star and disk formation – especially in the inner regions of protostellar disks – our simulations employ Adaptive Mesh Refinement (AMR). In this implementation, the grid is refined based on local physical conditions, most notably the Jeans length, λ_J, through the utilisation of the RAMSES code, which is defined as:

$$\lambda_J = \sqrt{\frac{\pi {c_s}^2}{G\rho}} \tag{2.10}$$

where c_s is the local sound speed. In accordance with the criterion established by Truelove et al. [59], it is imperative that the Jeans length has to be resolved by a minimum of 10 cells, with a view to averting the occurrence of artificial fragmentation. This means that the cell size Δx at a given refinement level l is :

$$\Delta x = \frac{L_{box}}{2^l} \tag{2.11}$$

where L_{box} is the size of the computational domain.

In order to ensure that even the heated inner regions of the disk are resolved with sufficient clarity, it is necessary to adopt a modified Jeans length:

$$\tilde{\lambda} = \begin{cases} \lambda_j, \text{if n} < 10^9 cm^{-3} \\ \min(\lambda_j, \lambda_j(T_{iso})), \text{if n} \geq 10^9 cm^{-3} \end{cases}$$

where $T_{iso} = 300K$ is a chosen isothermal threshold. This modification ensures that the disk's hot components are refined up to our maximum resolution – approximately 1.2 AU. The high resolution achieved via AMR is critical for resolving the internal structure of protostellar disks. With the grid dynamically refined, we are able to accurately model features such as radial surface density profiles, temperature gradients, and angular momentum distributions. This level of detail is essential for studying disk evolution, fragmentation, and the conditions that may lead to planet formation.

2.3.5 Extracting and Processing Ramses Data

RAMSES outputs are stored as binary files containing detailed information about the simulation's physical conditions, such as density, temperature, and velocity, across the AMR grid. In order to efficiently parse and visualise these data, two Python libraries are commonly employed: PyMSES and osyris. PyMSES is particularly effective for computational tasks, including ray tracing and data extraction, while osyris provides an intuitive interface for data visualisation. For the present study, PyMSES was utilised to extract the grid structures and relevant physical parameters from the binary files. The extracted data were then reformatted and prepared for further analysis. Furthermore, the selection of disks has been executed in a manner consistent with that employed for Lebreuilly 2021 [?]. The following criteria were applied to determine the inclusion of a gas cell l within the disk: - The cell's rotational velocity must exceed its radial fall velocity, $v_\phi > 2v_r$ - The cell's rotational velocity must exceed its vertical fall velocity, $v_\phi > 2v_z$ - The cell must be composed of dense material, $n > 10^9 cm^{-3}$, where n is the gas number density.

2.4 Comparative Analysis and Summary

The comparison between the phyisical assumption in the classic Bate model and in the new models highlights some key differences:

- **Angular momentum transport and fragmentation**: Bate's model, which is predominantly based on hydrodynamic and radiative processes, effectively resolves the fragmentation limit and forms discs and brown dwarfs in accordance with observations. However, the novel models demonstrate that the incorporation of a magnetic field significantly alters the transport of angular momentum, thereby influencing the occurrence of fragmentation, depending on the initial conditions.

- **Disc properties**: Bate's models provide a robust foundation for the establishment of correlations between disc mass, stellar mass and accretion. In the novel models, however, the incorporation of magnetic fields and protostellar outflows gives rise to variations in the size and masses of the discs, as well as exerting an influence on the relationships between disc parameters (e.g. surface density and radial profile).

- **Implications for planetary formation**: The comparison facilitates comprehension of the manner in which the extreme conditions simulated in the novel models (with MHD effects, feedbacks and outflows) can offer an alternative perspective to the classical case, thereby testing the robustness of the observed relationships and expanding our understanding of the processes that lead to the formation of planetary systems in low-mass environments.

Chapter 3

Comparative Analysis of Classical and Magnetized Simulation Results

In this chapter, a detailed comparison is presented between the classical hydrodynamical models developed by Bate (2008, 2011, 2018) and the new magnetohydrodynamical (MHD) simulations, incorporating non-ideal effects and additional feedback mechanisms. In order to facilitate a comparison between the models, a set of parameters were selected on the basis of their correlation with observables, including stellar mass, mass accretion rate, disk radius and disk mass. From an observational perspective, considerable effort has been invested in the acquisition of these data [57]. These considerations have also motivated Bate's choices; consequently, in the following chapter, a comparison will be made focusing on these parameters. The new models explore different physical regimes by varying key parameters. Specifically, we consider:

- **nmhd-in**: A simulation of a 1000 $M_\odot$ clump with a radius of 0.4 pc, a Mach number of 10, and a mass-to-flux ratio μ=10 (over the critical value). This model includes stellar radiative feedback but does not include protostellar jets.

- **nmhd-jets**: This model has the same initial conditions as nmhd-in, with the addition of a sub-grid treatment of protostellar jets.

- **nmhd-lowM**: Similar to nmhd-in, but with a clump mass of 500 $M_\odot$ (using the same radius, which results in a lower overall density).

- **nmhd-mu50**: Identical to nmhd-in except that the magnetic field is set to be five times weaker (i.e. $\mu = 50$)

The objective of this study is to assess the impact of magnetic fields, ambipolar diffusion, and protostellar jets on star and disk formation. To this end, a comparative analysis is conducted of the cumulative distributions of disk mass, disk radius, disk-to-star mass ratio, and time-averaged accretion rates among these models and with Bate's results.

This comparative analysis provides insights into the robustness of the theoretical framework across a range of physical conditions and helps bridge the gap between simulation predictions and observational data.

3.1 Stellar Mass Distributions

This plot 3.1 shows the cumulative fraction of stellar mass (on a logarithmic scale) for several models: Bate 2008, Bate 2011, and the new MHD/outflow models (`in`, `jets`, `lowM`, `mu50`). In addition, the mean, median and standard deviation for each model were computed, as illustrated in the following table 3.1. Bate (2008, 2011) simulations use an initial clump mass of 500 $M_\odot$. Notably, `lowM` also employs 500 $M_\odot$, while the other new models (e.g., `in`, `jets`, `mu50`) typically start with 1000 $M_\odot$. Despite this difference, the stellar mass distributions can still be compared to gauge the influence of additional physics. A clear shift is visible between the two curves of Bate's models, attributable to the inclusion of radiative transfer in Bate 2011. Radiative heating reduces excessive fragmentation, shifting the distribution toward somewhat higher masses and reducing the fraction of very low-mass objects. The new models (`in`, `jets`, `lowM`, `mu50`) do not exhibit dramatic differences among themselves in this stellar mass range. Their cumulative curves track each other relatively closely, indicating that while magnetic fields, outflows, or variations in initial mass can affect disk properties, the overall stellar mass distributions remain broadly consistent. Notably, the `jets` model aligns closely with Bate (2011), suggesting that when the initial mass and radiative transfer are similar, introducing protostellar jets does not drastically alter the stellar mass function, at least in the parameter space explored here. In summary, the stellar mass distribution plot underscores the importance of radiative transfer in shaping the IMF, as evidenced by the difference between Bate 2008 and 2011. Meanwhile, magnetic fields and outflows have less of an impact on the global mass function under these conditions, resulting in relatively small deviations among the new models.

Model	Mean	Median	Std
Bate 2008	0.1542	0.0721	0.2013
Bate 2011	0.6006	0.2205	0.8534
in	1.2006	0.5752	1.8996
jets	0.4108	0.2274	0.4850
lowM	0.6698	0.2930	0.9760
mu50	0.7999	0.3038	1.2062

Table 3.1: Mean, Median and Standard Deviation for each model in $M_\odot$.

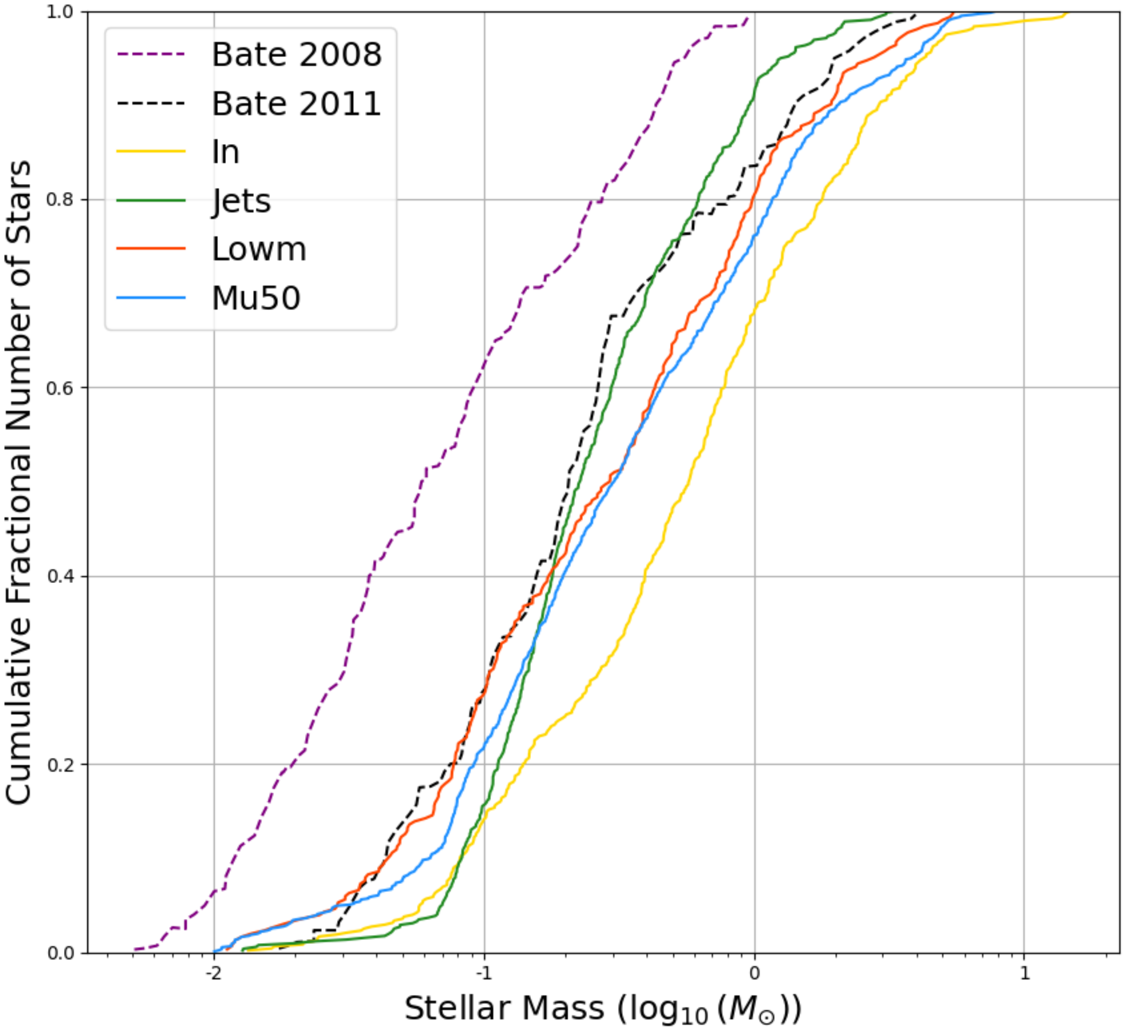

Figure 3.1: Cumulative fraction plot of stellar mass for different simulations.

3.2 Time Averaged Accretion Rate

In a multitude of theories concerning star formation, it is hypothesised that the accretion rate is proportional to the stellar mass. This is an observational constraint that emerges from the observation that the formation time scale is approximately independent of the final stellar mass. When expressed in log–log space, a slope of approximately 1 indicates a linear correlation In the course of the present simulations, higher slopes, approaching 1, were found to be in evidence, in comparison with the results obtained by Bate. This finding is consistent with the observations [57]. In this plot 3.2 we perform a linear regression fit for each model with SciPy tools. The following relation was used to compute the fit:

$$log(\dot{M}) = \alpha \log(M_\star) + \beta \tag{3.1}$$

The values obtained for each model are shown in the table 3.2. The `lowM` model (orange data points and orange dashed line) displays a high degree of alignment with the Bate (2011) model (red open circles and red dashed line). This similarity is attributable to the common origin of both simulations, which are initiated with a 500 $M_\odot$ clump, resulting in a comparable distribution of stellar masses and accretion behaviours. In the `mu50` model (illustrated by blue data points and blue dashed line), the magnetic field is five times weaker (μ=50) in comparison to the standard $\mu = 10$ configuration. This results in smaller stellar masses on average and lower accretion rates. This behaviour is consistent with the hypothesis that weaker magnetic fields provide less magnetic braking, but also alter the overall dynamics of collapse and mass distribution. As illustrated by the `in` (yellow data points and yellow dashed line) and `jets` (green data points and green dashed line) models, there is a high degree of similarity in the trends observed in both mass and accretion rate. This is evidenced by the linear fits, which demonstrate almost identical slopes. These findings suggest that the presence of protostellar jets does not result in a significant alteration of the mass–accretion rate relationship within the context of these initial conditions. Finally, all models demonstrate a positive correlation between stellar mass and accretion rate, consistent with theoretical predictions that more massive stars typically accrete at higher rates. However, the scatter and the best-fit slopes deviate marginally, underscoring the influence of magnetic field strength and initial clump mass in determining accretion properties.

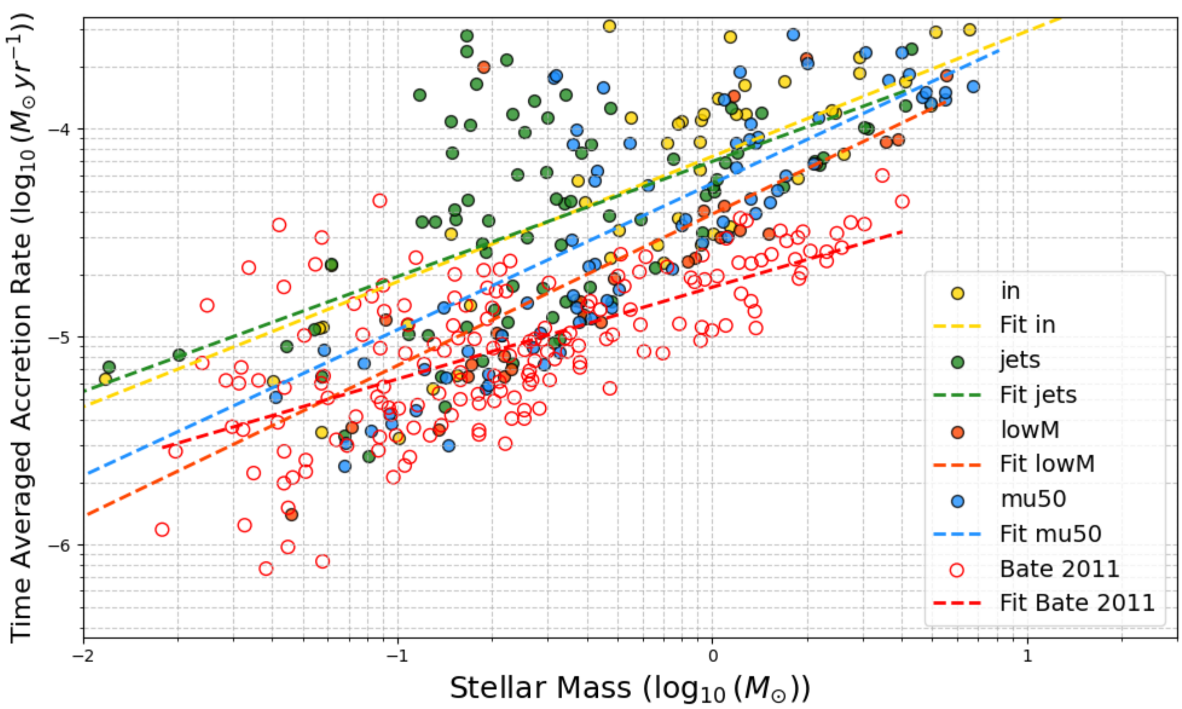

Figure 3.2: Scatter plot of stellar mass vs. time averaged accretion rate with best-fit lines.

Model	Slope (α)	Intercept (β)	R^2 value
Bate 2011	0.442 ± 0.039	-4.762 ± 0.033	0.428
in	0.602 ± 0.042	-4.133 ± 0.052	0.776
jets	0.554 ± 0.061	-4.157 ± 0.069	0.481
lowM	0.728 ± 0.048	-4.410 ± 0.087	0.841
mu50	0.703 ± 0.049	-4.263 ± 0.054	0.707

Table 3.2: Slope, Intercept and R^2 value for the fit of each model.

3.3 Disk Mass Distributions

These panels 3.3 show the cumulative fraction of disk masses (logarithmic scale) for various stellar mass bins. The top-left panel combines all stellar masses, while the top-right, bottom-left, and bottom-right panels focus on $M_\star < 0.1M_\odot, 0.1 \geq M_\star \leq 0.3M_\odot$, and $M_\star > 0.3M_\odot$, respectively. The accompanying table shows the number of points for each model and mass range 3.3. We compare the new MHD/outflow models (`in`, `jets`, `lowM`, `mu50`) against Bate (2018), which includes radiative transfer and starts with a 500 $M_\odot$. In the top-left panel (all stellar masses combined), the distributions for most models overlap significantly at lower disk masses but begin to diverge at the higher end. This divergence reflects how disk growth can be affected by factors like magnetic fields and outflows. As illustrated in the top-right panel, there is a negligible variation among the models in this substellar regime. The curves are distributed in a relatively dense pattern, suggesting that brown dwarfs (or very low-mass stars) characteristically form disks of analogous mass, irrespective of the particular physics incorporated. However, Bate (2018) has produced results that are somewhat at odds with the rest of the data set, as he has observed a tendency for slightly less massive disks in this low-mass range. This suggests the possibility that radiative feedback or initial conditions in Bate's setup may suppress disk mass growth more effectively at the brown dwarf scale. As the focus shifts towards more massive stars, the disparities amongst models become increasingly evident. For instance, `mu50` demonstrates a pronounced deviation from the other runs, suggesting that a weaker magnetic field may result in systematically distinct (often larger) disk masses. The results obtained demonstrate that, while radiative feedback (as in Bate 2018) can suppress disk masses at lower stellar masses, the strength of the magnetic field becomes increasingly influential at higher stellar masses, thereby creating a broader spread in disk mass distributions among the new models.

Model	$< 0.1M_\odot$	$0.1 - 0.3M_\odot$	$> 0.3M_\odot$	tot.
in	69	122	541	732
jets	61	600	267	928
lowM	20	27	100	147
mu50	171	297	957	1425

Table 3.3: Number of points for each massa range in the distributions plots

3.4 Disk Radius Distributions

These panels 3.4 show the cumulative fraction of disk radii (logarithmic scale) for various stellar mass bins. The top-left panel includes all stellar masses, while the other three panels focus on $M_\star < 0.1M_\odot, 0.1 \geq M_\star \leq 0.3M_\odot$, and $M_\star > 0.3M_\odot$. In the top-left panel, `mu50` (blue dotted line) tends to produce more extended disks (shifted to the right), whereas `lowM` (orange-dotted line) yields systematically smaller disks (shifted to the left). Bate (2018) (solid black) aligns closely with the `in` (yellow) and `jets` (green) models, suggesting that for an initial clump of 500 $M_\odot$ the presence of moderate magnetic fields or outflows does not drastically alter the global disk size distribution in these runs. Focusing on the top-right panel, we again see`mu50` forming larger disks, while Bate (2018) is shifted left, indicating smaller disk radii. Interestingly, Bate (2018) is even smaller than lowM in this brown dwarf regime, a deviation from the pattern seen in the other mass bins, where Bate (2018) and lowM often cluster more closely. The bottom panels show a similar trend: `mu50` remains shifted to the right (indicating larger disk radii), while `lowM` tends to the left. Bate (2018), `in`, and `jets` generally overlap, reinforcing that their disk sizes are comparable across these stellar mass ranges. Overall this figure indicates that the magnetic field strength and initial mass distribution are pivotal in determining disk radii, with `mu50` showing a marked effect on disk sizes. Furthermore, the concurrence of results between Bate (2018), `in`, and `jets` suggests that moderate alterations in feedback physics (e.g., outflows) do not significantly impact disk radii, with the exception of specific regimes such as brown dwarf formation, where radiative feedback can exert a more substantial effect.

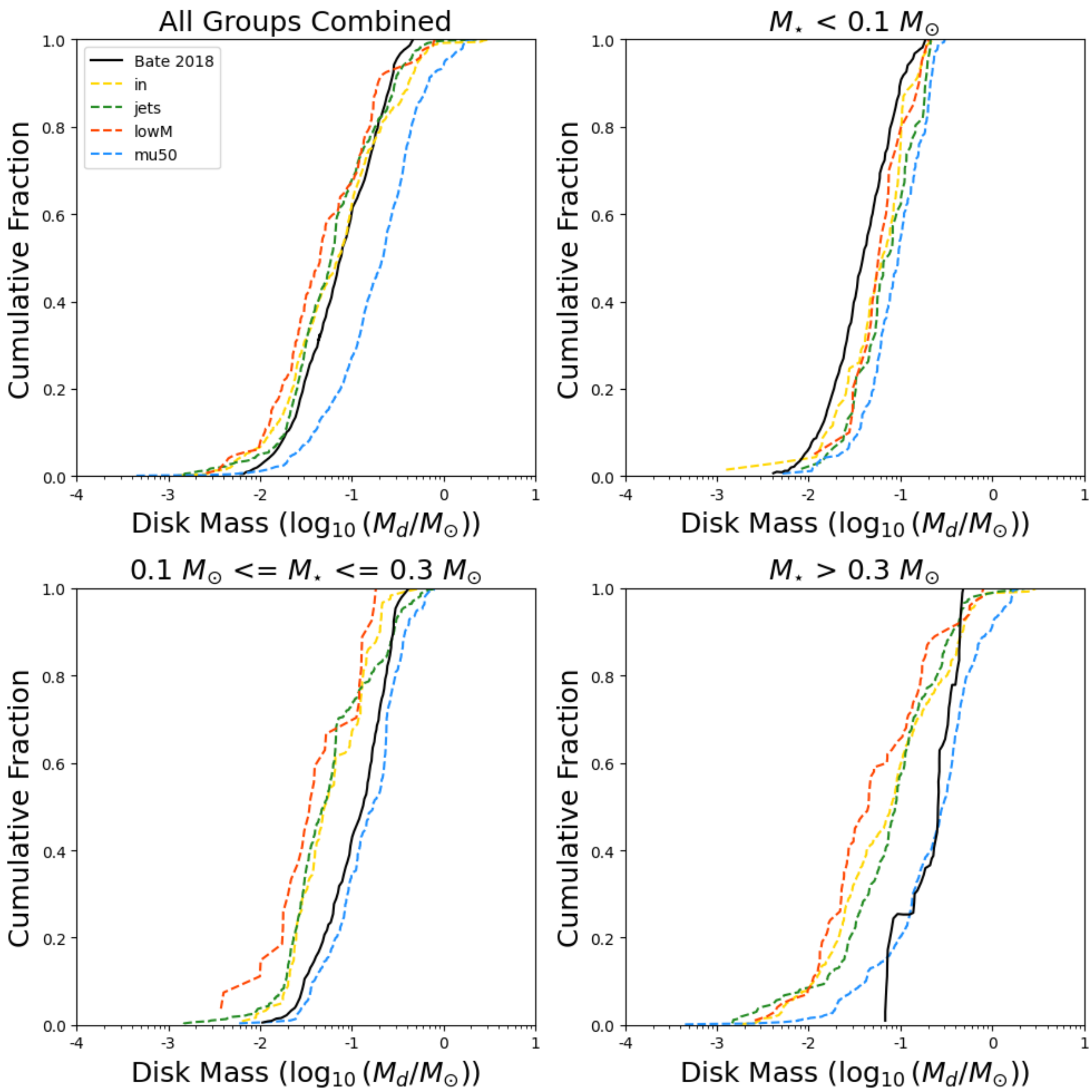

Figure 3.3: Cumulative fraction of disks as a function of their mass for different stellar mass bins.

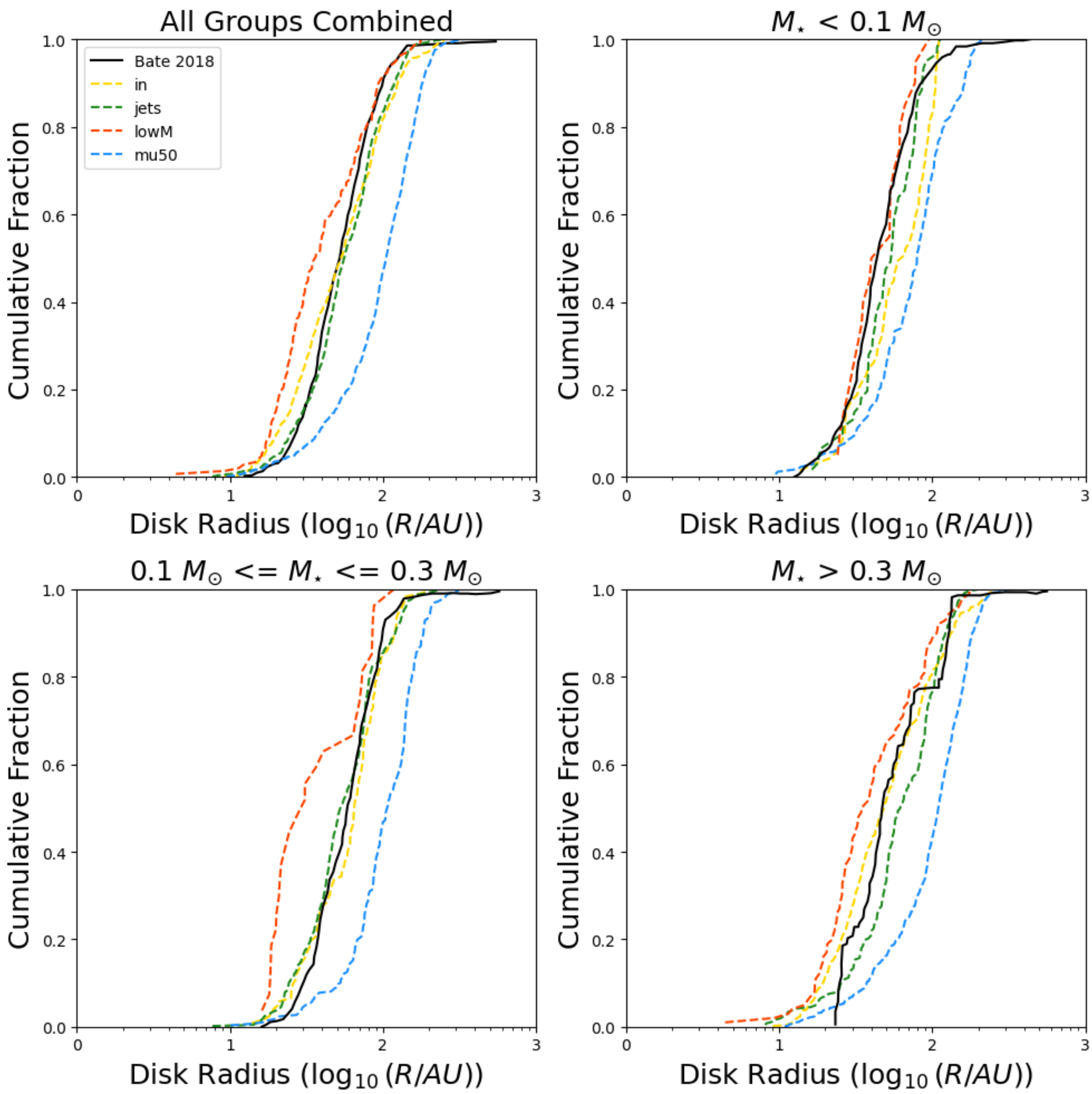

Figure 3.4: Cumulative fraction of disks as a function of their radius for different stellar mass bins.

3.5 Disk-to-Star Mass Ratio

These plots (3.5) display the cumulative fraction of the ratio between disk mass and stellar mass (on a logarithmic scale). The top-left panel includes all stellar masses combined, while the other three panels isolate the brown dwarf regime, intermediate masses and and higher masses. Two vertical gray lines mark the gravitational stability thresholds at ratios of 0.3 and 1. In the combined plots, Bate (2018) (black curve) tends to yield higher disk-to-star mass ratios overall, with the majority of its disks lying between 0.3 and 1. In contrast, the new models (`in jets`, `lowM`, and `mu50`) have systematically lower ratios, indicating that the majority of their disks are well below 0.3. This suggests a reduced disk mass relative to the stellar mass and more stable disks against gravitational instability. In the Brown Dwarf Regime, all new models produce larger disk-to-star mass ratios compared to Bate (2018). In many cases, they remain within the 0.3–1 band. An exception is `mu50`, which continues to lie mostly outside the stability boundaries, indicating that a weaker magnetic field can allow for more massive disks relative to the (very low-mass) star, pushing to high mass ratios and thus to gravitational instability. Fot Intermediate and Higher Mass Stars, the new models remain at comparatively low ratios, reinforcing the trend seen in the all-masses panel. The main outlier continues to be `mu50`, which sporadically shifts toward higher ratios, often exceeding the 1.0 threshold, indicating gravitationally unstable conditions. The objective of the analysis is to ascertain whether a significant proportion of protostellar disks may induce planet formation through gravitational instability. It is infrequent to observe disk fragmentation in these simulations, as these young disks are extremely hot and accreting onto the central star at high rates.

3.6 Brown Dwarf Disks: Mass Variations and Stability Trends

In conclusion, the brown dwarf regime is of particular interest, as its formation dynamics show distinct behaviour compared to those of more massive stellar objects. The data presented indicate that, although the MHD and classical simulations show convergence in the distribution of overall stellar masses, significant discrepancies are observed in the case of brown dwarfs. With regard to the disk mass distribution graph, a significant variation becomes evident: within the brown dwarf regime, the disks are systematically more massive than those predicted by the Bate model, whilst for higher-mass stars the disks are generally less massive, with the exception of the mu50 model, which maintains a higher disk mass. Concurrently, analysis of the disk-to-star mass ratio demonstrates that, within the substellar regime, the majority of disks are stable (i.e. within the gravitational stability zone). Conversely, in other mass ranges, there is a tendency for disks to move outside this zone.

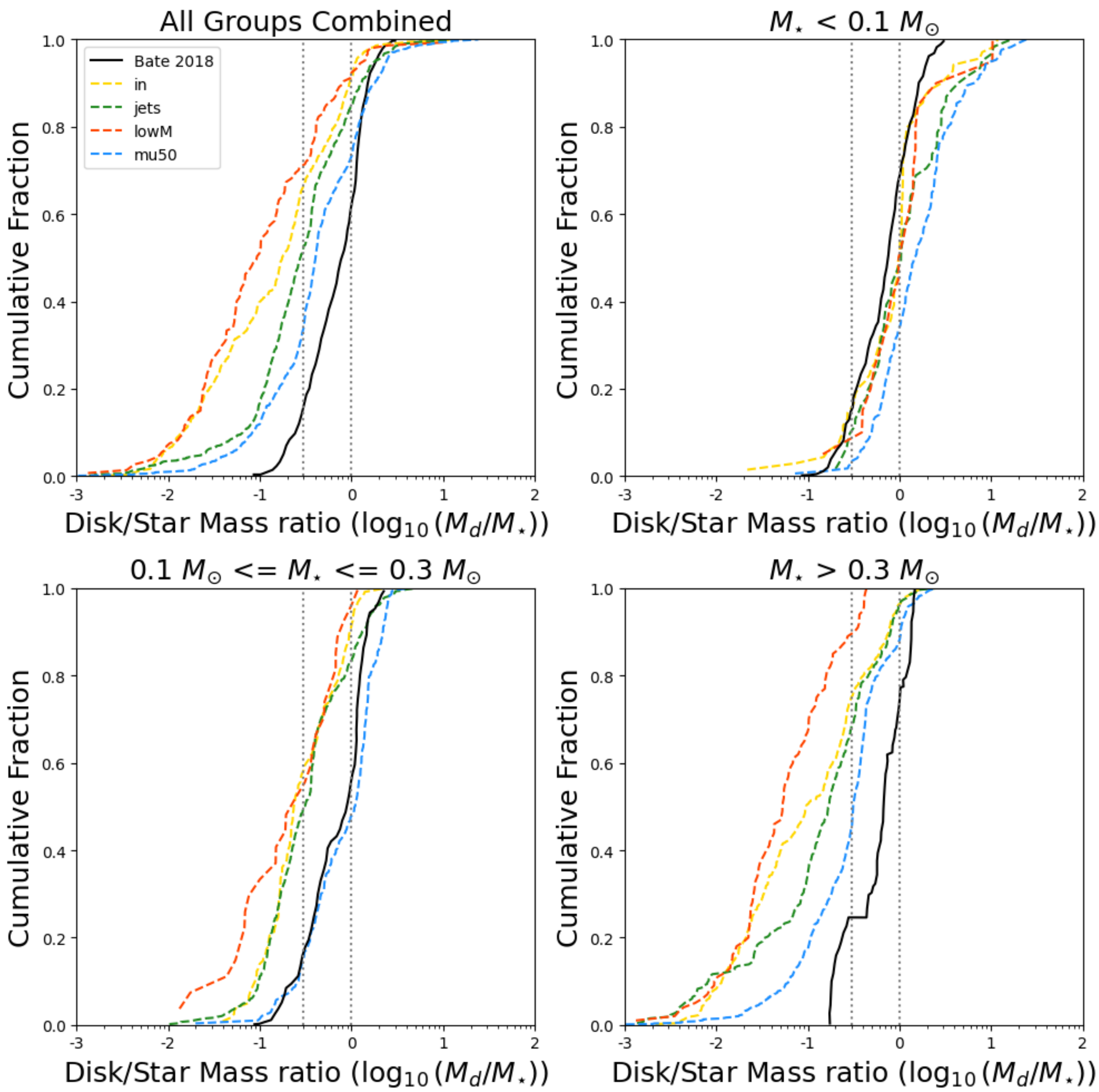

Figure 3.5: Cumulative fraction of disks as a function of their disk to stellar mass ratio for different stellar mass bins.

These results underscore the intricacy of the mechanisms governing the formation of brown dwarfs. They also highlight the necessity for additional research to comprehensively grasp the variations in behaviour as a function of mass, with particular emphasis on the combined effects of radiative feedback, magnetic force, and initial conditions.

3.7 Concluding Remarks

This chapter provides a detailed comparative analysis of the classical hydrodynamical simulations by Bate (2008, 2011, 2018) and the new magnetohydrodynamical (MHD) simulations that incorporate non-ideal effects and additional feedback mechanisms. The following key points have been identified through this analysis:

- **Stellar Mass Distributions:** The incorporation of radiative transfer in Bate (2011) led to a reduction in excessive fragmentation and a shift in the stellar mass distribution towards slightly higher values. Despite the MHD simulations (`in`, `jets`, `lowM`, `mu50`) commencing from disparate initial clump masses, their stellar mass distributions remain largely comparable. This observation suggests that the inclusion of magnetic effects and feedback does not significantly alter the overall shape of the initial mass function (IMF), even if the total number of stars fomred is very different.

- **Accretion Rates:** The investigation of time-averaged accretion rates, expressed in log–log space, has confirmed a positive correlation with stellar mass across all models. Variations in the best-fit slopes indicate that both the magnetic field strength and the initial clump density can influence the detailed dynamics of the accretion process.

- **Disk Properties:** The cumulative distributions of disk mass and radius, in conjunction with the disk-to-star mass ratios, demonstrate marked variations among the models. Specifically, a weaker magnetic field (as observed in the `mu50` model) tends to result in more extended disks, and in certain instances, disks that are more massive relative to the star, potentially leading to gravitational instability. Conversely, the inclusion of protostellar jets (as in the `jets` model) does not appear to significantly alter disk properties, thereby underscoring the dominant role of initial conditions and radiative feedback.

- **Theoretical and Observational Implications:**The findings serve to reinforce the robustness of the classical theoretical framework, thereby demonstrating that while classical models provide reliable predictions for stellar mass distributions, incorporating MHD effects offers a more detailed understanding of disk formation and initial evolution.The integration of simulations and observational data is therefore essential for the refinement of theories of star and planet formation.

In conclusion, a comparison between classical and magnetised simulations has been made, highlighting the key parameters – radiative transfer, magnetic field strength, and the presence of jets – that modulate both stellar formation and disk structure. These findings represent a significant step towards bridging theoretical models with observational evidence, offering valuable insights for further studies aimed at a deeper understanding of the underlying mechanisms in star and planet formation. It is evident that disk properties are contingent on physics; therefore, the initial condition for planet formation is also subject to this influence. The available mass, density, and size of the disk are particularly pertinent in this regard. A thorough analysis of these properties is imperative to comprehending the processes of planet formation, the role of gravitational instability and the subsequent disk evolution.

Chapter 4

Analysis of the New MHD Simulation Results

In this chapter, we present an in-depth analysis of simulation data from the new ECOGAL RAMSES magneto-hydrodynamical models. The present study starts with an investigation into the relationship between disk mass and stellar mass, with a view to examining the manner in which this correlation evolves over time. Thereafter, the specific accretion rate is explored as a function of stellar mass, with linear fits performed on logarithmic scales for each model in order to accurately capture the underlying trends. Subsequently, an analysis is conducted of the temporal evolution of several key disk properties, namely the distributions of disk radius, disk mass, and the disk-to-star mass ratio across all four models. Thereafter, the focus is shifted to the disk's surface density, where an examination is made of its dependence on critical parameters such as stellar mass and the magnetic field parameter, beta. Finally, the focus is shifted to an in-depth exploration of the relationships between the beta parameter and other disk parameters. This investigation aims to elucidate the influence of magnetic fields on disk formation and evolution. Through this comprehensive analysis, the chapter seeks to enhance our understanding of the interplay between disk properties and magneto-hydrodynamical effects in star-forming regions. We also identify trends and properties that can be probed observationally to constrain models.

4.1 Comparative Analysis of the Disk Mass–Stellar Mass Relationship in MHD Models

The series of graphs 4.1, 4.2, 4.3, 4.4, 4.5 illustrates the evolution of the disk mass–stellar mass relationship over four distinct time snapshots, as well as in an overall integrated view. As time progresses, it is evident that the data points shift to the right along the stellar mass axis. This tells us that the number of massive stars is increasing.

A robust positive correlation between disk mass and stellar mass persists across all times, indicating that, at any given stage, more massive stars tend to host more massive disks. This is because the disk-star system continues to accumulate mass infalling from the clump as the stellar mass forms. In order to quantify the relationship between these variables, a logarithmic fit was applied to the data, using the following relation:

$$log(\dot{M}_d) = \alpha \log(M_\star) + \beta \tag{4.1}$$

The resulting parameters for the aggregated data can be found in the accompanying table 4.4. For the `lowM` model, the analysis reveals a distinct evolution in the correlation between disk mass and stellar mass. At the early stages (10 and 20 kyr), there is a strong negative correlation, suggesting that initially, as stellar mass increases, the corresponding disk mass decreases—likely due to rapid early-stage processes such as aggressive accretion or disk depletion. However, at later times (30 and 40 kyr), this trend shifts toward a positive correlation, aligning with the expected behavior where more massive stars tend to harbor more massive disks. The relation between disk mass and stellar mass depends on physical properties such as magnetic field and density, as well as time, so understanding clump dispersion is crucial to deriving an accurate ratio at the end of the protostellar phase. Furthermore, the observed overall trend indicates a decrease in disk mass over time, thereby reinforcing the hypothesis that stellar processes, including photoevaporation and accretion, gradually erode the disk material. The present findings are consistent with those of previous studies, which have demonstrated a similar evolutionary behaviour in the more evolved protoplanetary disks [6]. Furthermore, the temporal evolution depicted by these graphs emphasises the necessity of incorporating time-dependent feedback mechanisms into magneto-hydrodynamical simulations, thereby facilitating more precise replication of the intricate interactions that govern disk dissipation in star-forming regions.

Model	Slope (α)	Intercept (β)	R^2 value
10 kyr	0.0307 ± 0.0755	-1.2096 ± 0.0549	0.0009
20 kyr	0.1500 ± 0.0652	-1.0547 ± 0.0407	0.0307
30 kyr	0.1561 ± 0.1007	-1.1247 ± 0.0576	0.0241
40 kyr	0.8017 ± 0.3125	-1.1498 ± 0.1754	0.1960
	0.1675 ± 0.0423	-1.0931 ± 0.0275	0.0321

Table 4.1: Slope, Intercept and R^2 value for the fit of for the model "in".

Model	Slope (α)	Intercept (β)	R^2 value
10 kyr	0.3894 ± 0.0898	-0.8429 ± 0.0750	0.0888
20 kyr	-0.1012 ± 0.1134	-1.1621 ± 0.0777	0.0043
30 kyr	0.0321 ± 0.1212	-0.9398 ± 0.0760	0.0006
40 kyr	0.1060 ± 0.3064	-0.8675 ± 0.1511	0.0052
	0.1694 ± 0.0580	-0.9705 ± 0.0422	0.0164

Table 4.2: Slope, Intercept and R^2 value for the fit of for the model "jets".

Model	Slope (α)	Intercept (β)	R^2 value
10 kyr	-0.2313 ± 0.0661	-1.4887 ± 0.0791	0.1908
20 kyr	-0.3719 ± 0.0878	-1.3971 ± 0.0756	0.1521
30 kyr	0.1820 ± 0.0982	-0.9000 ± 0.0663	0.0384
40 kyr	0.2114 ± 0.1660	-1.1322 ± 0.0856	0.0282
	-0.0142 ± 0.0479	-1.1222 ± 0.0398	0.0003

Table 4.3: Slope, Intercept and R^2 value for the fit of for the model "lowM".

4.2 Specific Accretion Rate Trends in MHD Simulations

In the initial plot 4.6, the slope values of the logarithmic fits for the instantaneous accretion rate across the four MHD models are demonstrated, with these models divided into two stellar mass ranges and an overall aggregated dataset. The aggregated fits demonstrate analogous slopes among all models, thus indicating a broadly consistent relationship between stellar mass and accretion rate when the full mass range is considered. However, a clear distinction emerges when the sample is divided according to stellar mass. Specifically, for lower-mass stars ($M_\star < 0.25 M_\odot$), the `jets` and `mu50` models demonstrate significantly lower slopes in comparison to the `in` and `lowM` models. This finding indicates that outflows (`jets`) and weaker magnetic fields (`mu50`) may exert a more substantial influence on accretion behaviour in very low mass stars and brown dwarfs. Moreover, the `jets` model is particularly salient for higher-mass stars ($M_\star > 0.25 M_\odot$). This model exhibits a marked change in slope relative to the other models, indicating that protostellar jets could have a pronounced impact on accretion in the upper mass range. The second plot 4.7, which presents all the data points and their respective fits, provides further confirmation of the agreement among the aggregated fits across the four models. The final fit values obtained for the entire dataset are summarised in the accompanying table4.5. Usually from observations we find a value

Model	Slope (α)	Intercept (β)	R^2 value
10 kyr	0.2867 ± 0.0499	-0.6624 ± 0.0472	0.1329
20 kyr	0.0262 ± 0.0326	-0.7539 ± 0.0270	0.0018
30 kyr	0.1850 ± 0.0509	-0.5779 ± 0.0325	0.0521
40 kyr	0.1031 ± 0.1080	-0.6928 ± 0.0603	0.0096
	0.1594 ± 0.0236	-0.6722 ± 0.0186	0.0479

Table 4.4: Slope, Intercept and R^2 value for the fit of for the model "mu50".

for the slope close to 1, but at later times we see that the slope can reach values up to 1.3-1.5 [57]. The only model that reaches these values is the `jet model`, so it may be useful to pursue this in future studies.

Model	Slope (α)	Intercept (β)	R^2 value
in	0.818 ± 0.038	-9.601 ± 0.058	0.502
jets	0.818 ± 0.053	-10.132 ± 0.091	0.328
lowM	0.681 ± 0.048	-10.025 ± 0.095	0.408
mu50	0.755 ± 0.024	-9.695 ± 0.046	0.522

Table 4.5: Slope, Intercept and R^2 value for the fit of each model.

4.3 Age-Dependent Cumulative Distributions of Disk Mass, Radius, and Disk-to-Star Mass Ratio

The cumulative distributions of disk mass 4.8 indicate a clear temporal evolution, with disk masses generally shifting to lower values over time. This is not so obvious by the moment we are at the early stages of disc formation and there's still accretion from the clump. In contrast, the disk radius distributions 4.9 show no pronounced temporal variation, although `mu50` again tends to form larger disks. The observed stability in disk radii, despite the decreasing mass, suggests that the average disk density is diminishing over time. Finally, the cumulative distributions of the disk-to-star mass ratio 4.10 reveal that, as time progresses, disks progressively become more stable. This observation lends further support to earlier findings from comparisons with Bate's models, emphasizing that these MHD simulations generate more stable disks in general. Anyway it is clear that the `lowM` and `mu50` models are characterized by the production of larger disk-to-stellar mass ratios, a property that is concomitant with an increase in the degree of instability. A salient finding of these plots is that they facilitate the discernment of the models and their underlying physics by observing the evolution of these quantities.Indeed,

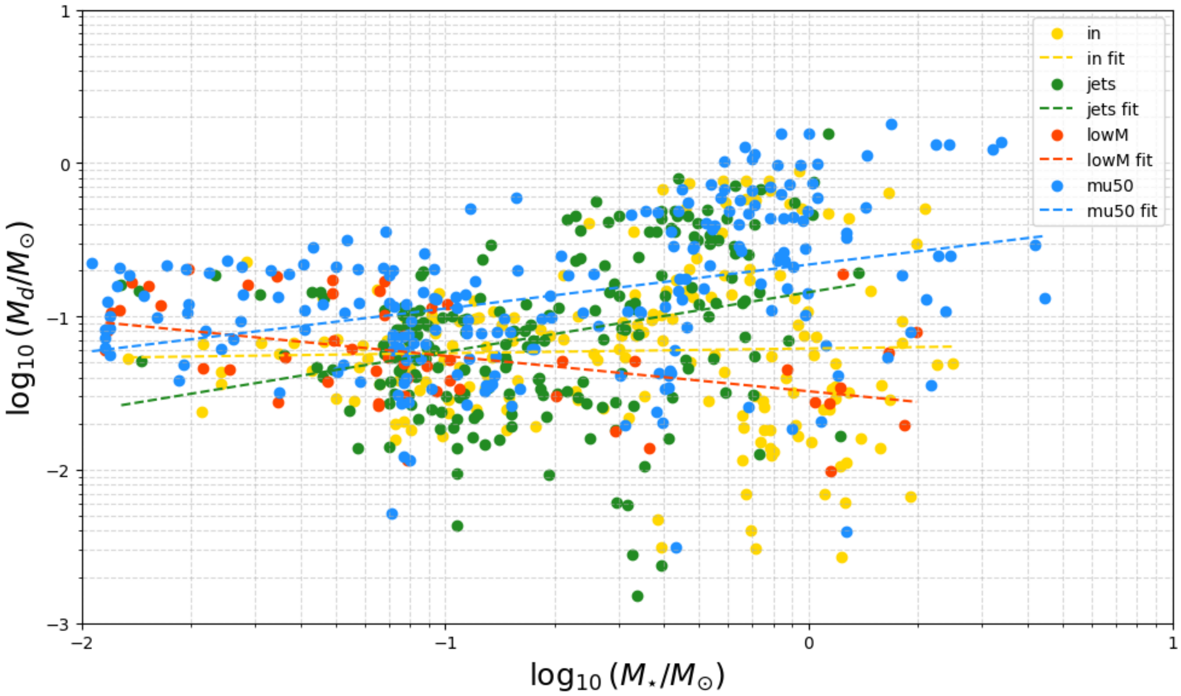

Figure 4.1: Disk mass versus stellar mass at 10 kyr.

the `mu50` model (which possesses a weaker magnetic field) frequently exhibits curves that shift towards higher values of disc mass or disc radius (and consequently disc mass to star ratio), especially at higher ages. This observation is consistent with the hypothesis that a weaker magnetic field exerts a lesser restraint on the formation and growth of discs, thereby allowing for the formation of more massive and/or larger discs. The remaining three models, characterized by a more pronounced magnetic field, typically exhibit less substantial or less extensive discs, particularly in the initial stages of evolution. This is attributable to the fact that the transportation of angular momentum by the magnetic field and jets/outflows tends to diminish the size and mass of the disc.

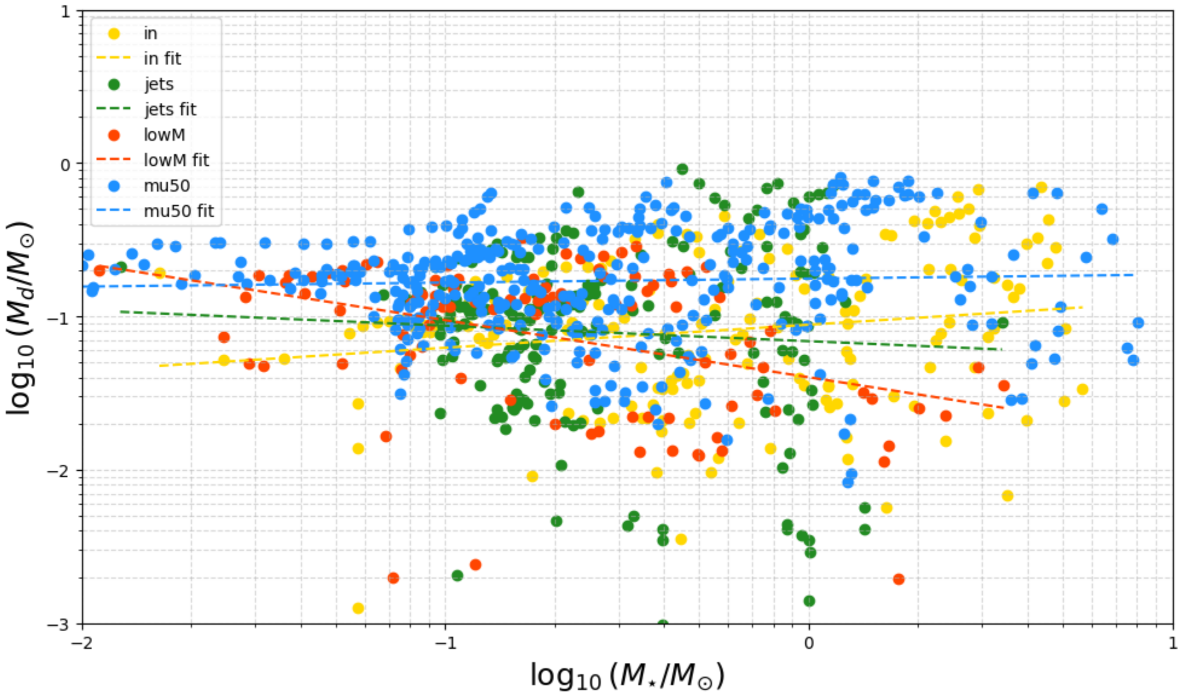

Figure 4.2: Disk mass versus stellar mass at 20 kyr.

4.4 Surface Density Distributions and Their Evolution Across Stellar Mass Bins

In the following plot 4.11 the surface density distributions for each of the four models are presented. For each distribution, lines representing the mean, median, and the 16th and 84th percentiles have been included in order to capture the statistical trends. The evolution of the density distributions demonstrates a lack of significant differences among the models, as evidenced by the close agreement observed in the total distribution. However, the `mu50` model produces a considerably higher number of disks, even if they are more unstable. Furthermore, in contrast to the other models that demonstrate a discernible decline in surface density over time (as evidenced by the mean values), the `mu50` model exhibits no significant decrease in density. The plots showing the global evolution in time and for different mass ranges can be found in the appendix. In the second graph, 4.12 the surface density is plotted as a function of stellar mass at the four specified time points. For each model at every time point, a logarithmic fit has been performed, and the corresponding fit lines are overlaid on the plots, highlighting the evolution of this relationship. A very interesting trend emerges: over time, a clear correlation between the disk surface density and stellar mass is developed. At the earliest stages, however, there is little to no correlation, as evidenced by an almost zero slope. However, as the

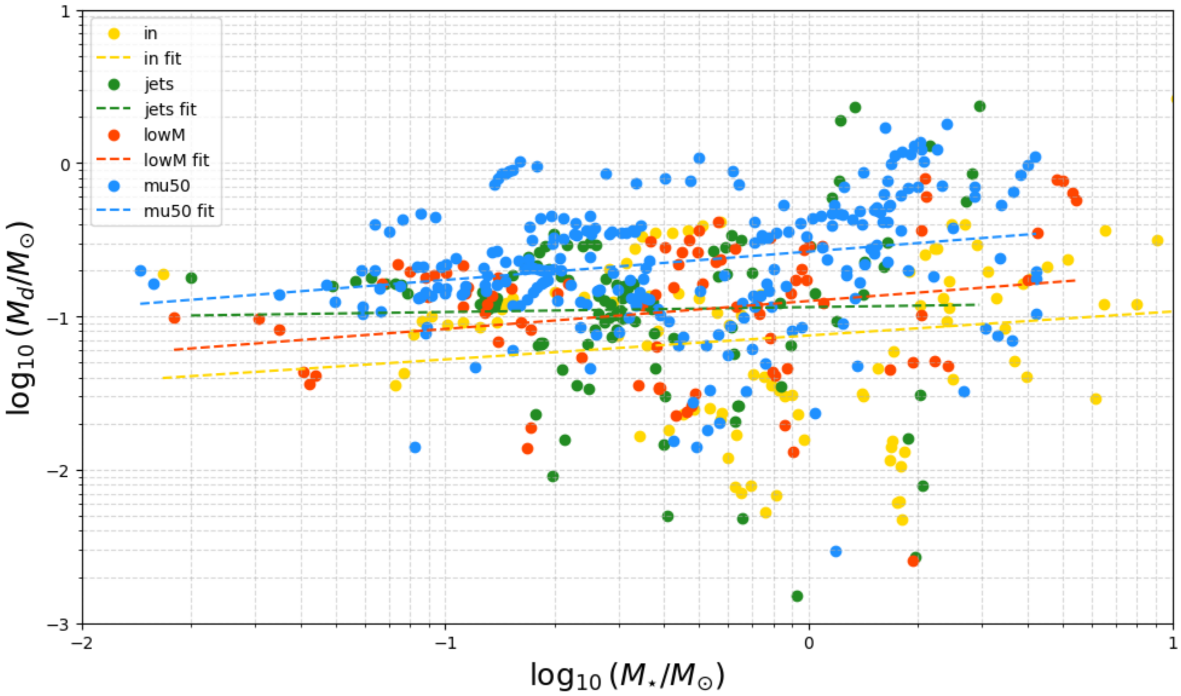

Figure 4.3: Disk mass versus stellar mass at 30 kyr.

temporal progression progresses, a discernible correlation becomes evident, with slope values ranging from 0.2 to 0.4, thereby suggesting that higher-mass stars are more likely to host disks characterised by higher surface densities. This phenomenon may be attributable to the interplay between the inflow from the clump and the accretion onto the star as a function of mass. This phenomenon cannot be traced in current simulations, but it will be the subject of future study with tracer particles.

4.5 Brown Dwarf Disk Radii: Comparing Mass and Magnetic Field Effects

The histogram under consideration here 4.13 highlights the distribution of disk radius for brown dwarfs in four different models. It is noteworthy that the `in` and `jets` runs exhibit a remarkably similar distribution, with a tendency towards smaller disk radii. Conversely, `mu50` and `lowM` demonstrate a predominance of larger disks. These observations imply that decreasing either the initial clump mass (`lowM`) or the magnetic field strength (`mu50`) can result in analogous outcomes for brown dwarf disks. This phenomenon can be attributed to the reduced disk density observed for `lowM`, and to the diminished magnetic breaking exhibited by `mu50`. The incorporation of jets appears to exert a lesser influence

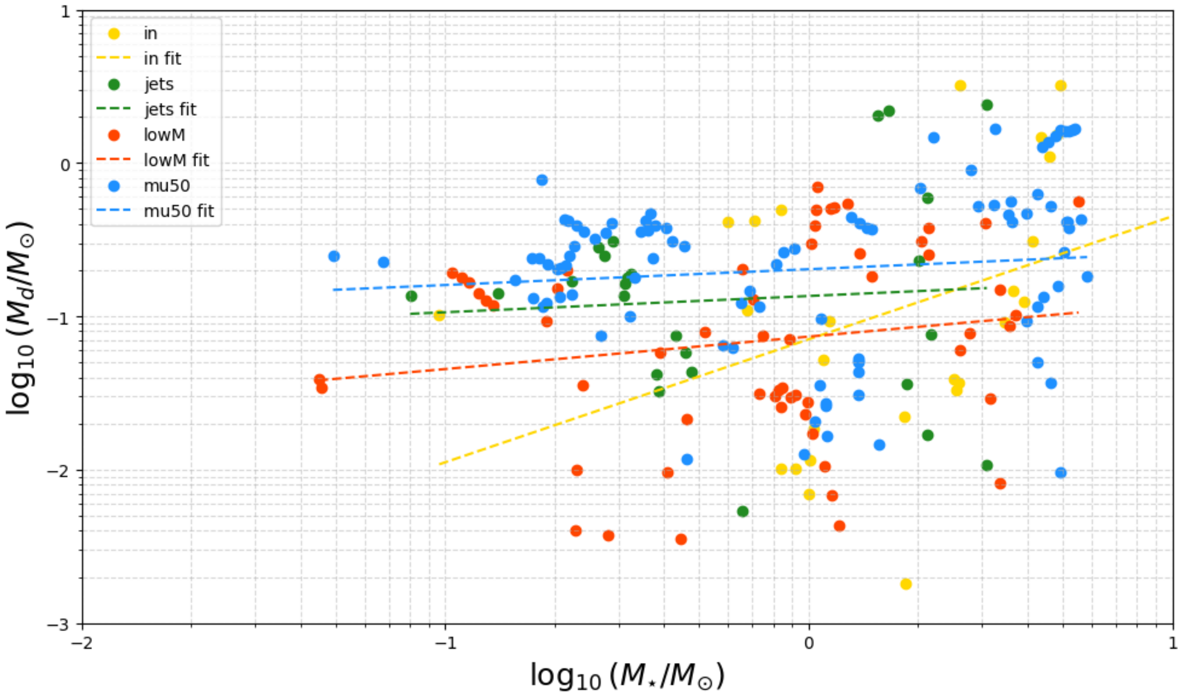

Figure 4.4: Disk mass versus stellar mass at 40 kyr.

on their ultimate sizes. It is evident that feedback processes such as jets are incapable of injecting angular momentum into the clump to recover the effects of the magnetic field.

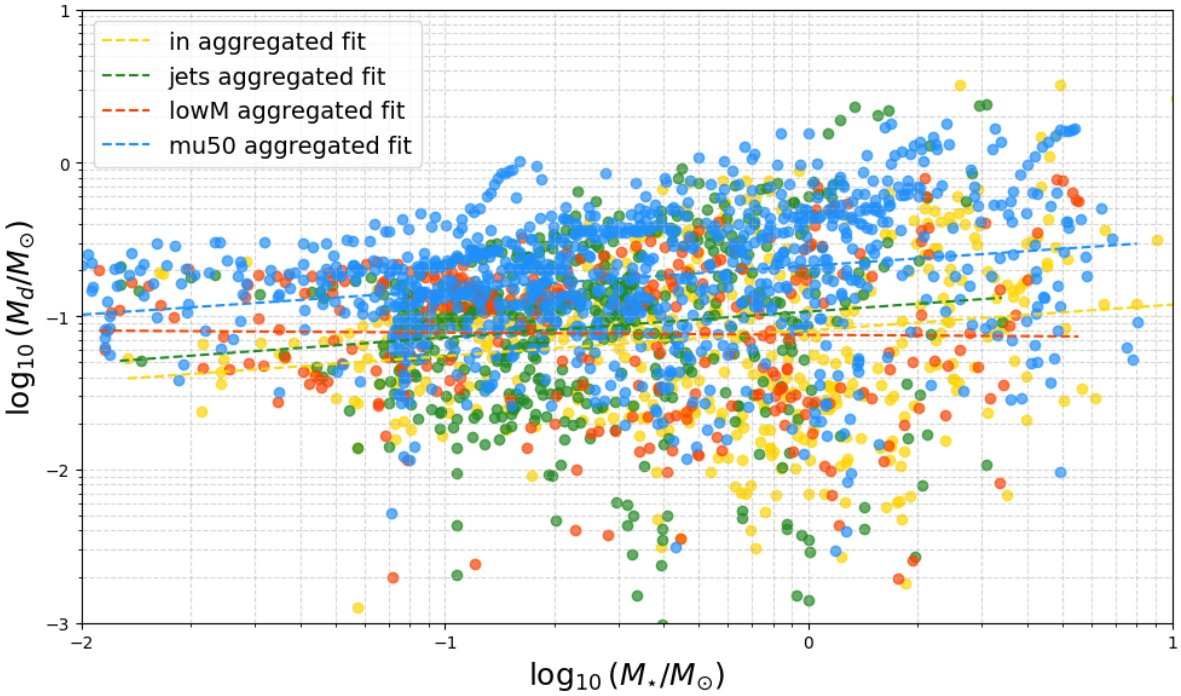

Figure 4.5: Overall disk mass–stellar mass relationship for the four MHD models, integrated over the entire simulation period.

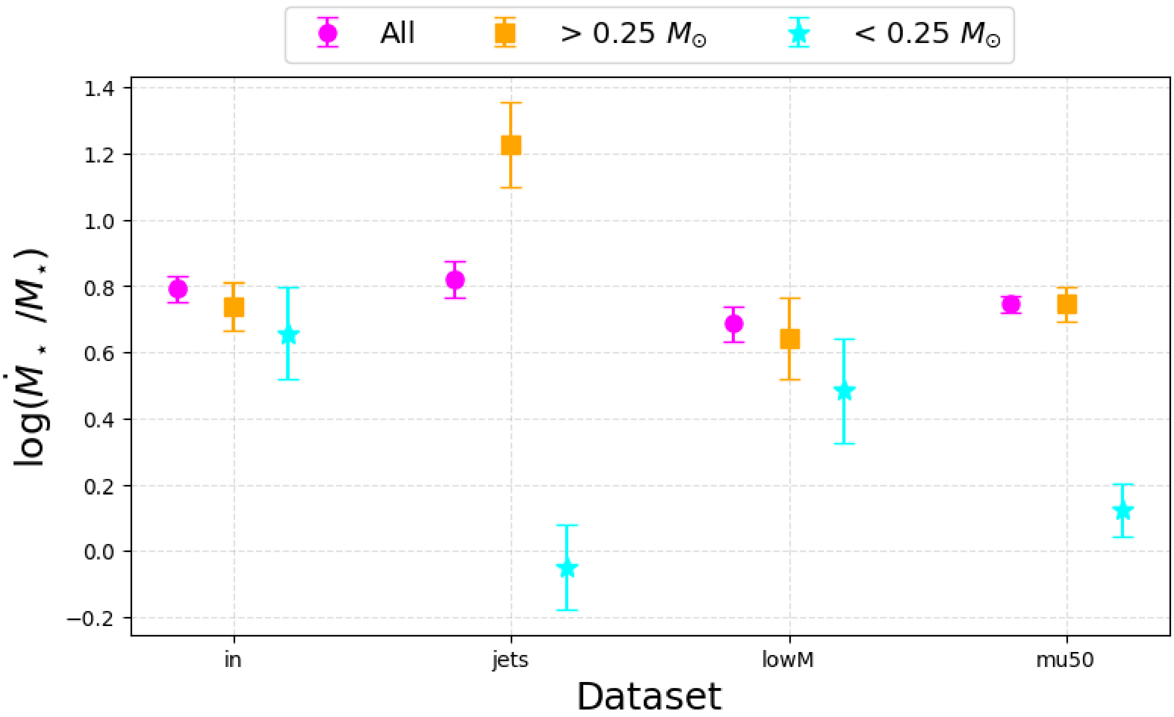

Figure 4.6: Logarithmic fit slopes for the instantaneous accretion rate across the four MHD models, analyzed by stellar mass ranges and as an aggregated dataset.

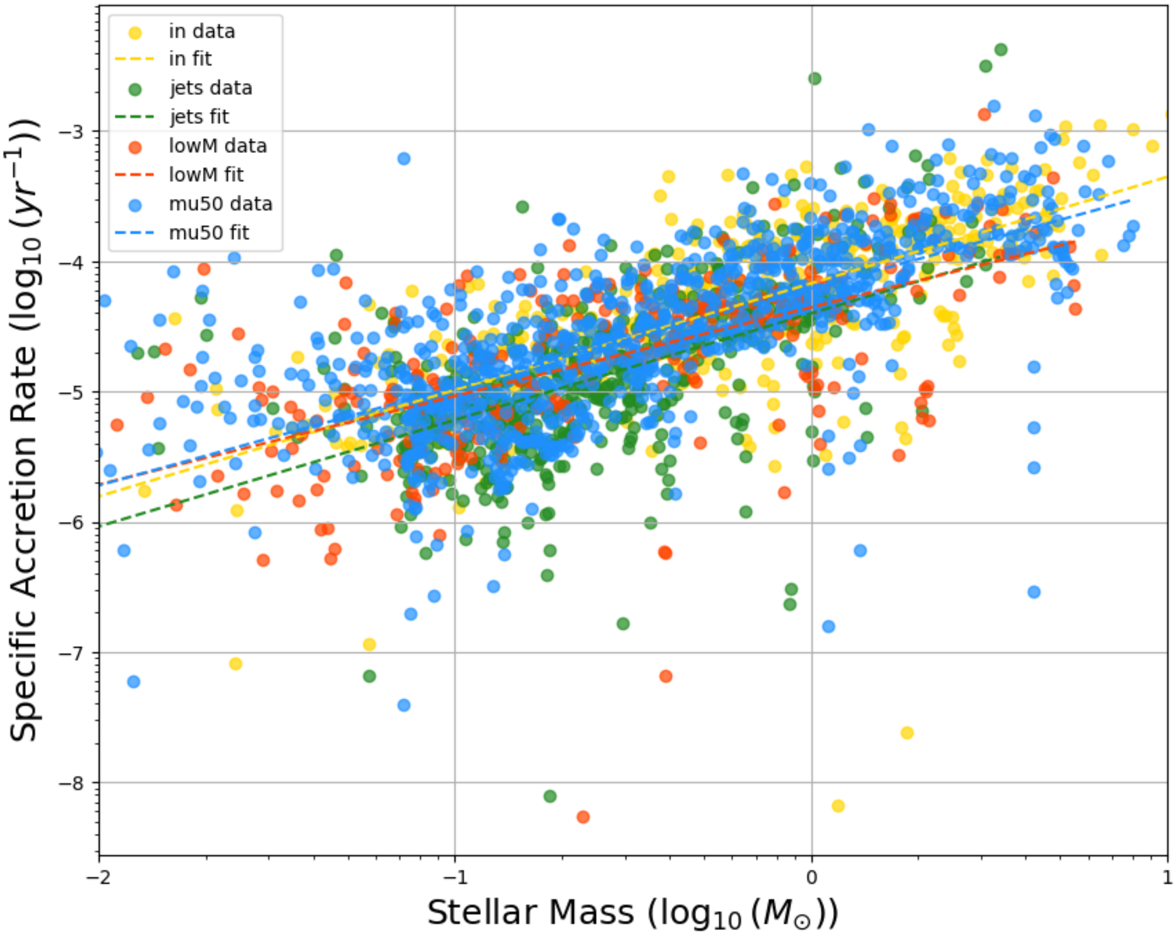

Figure 4.7: Scatter plot displaying all data points and their respective logarithmic fit lines for the instantaneous accretion rate in the four MHD models.

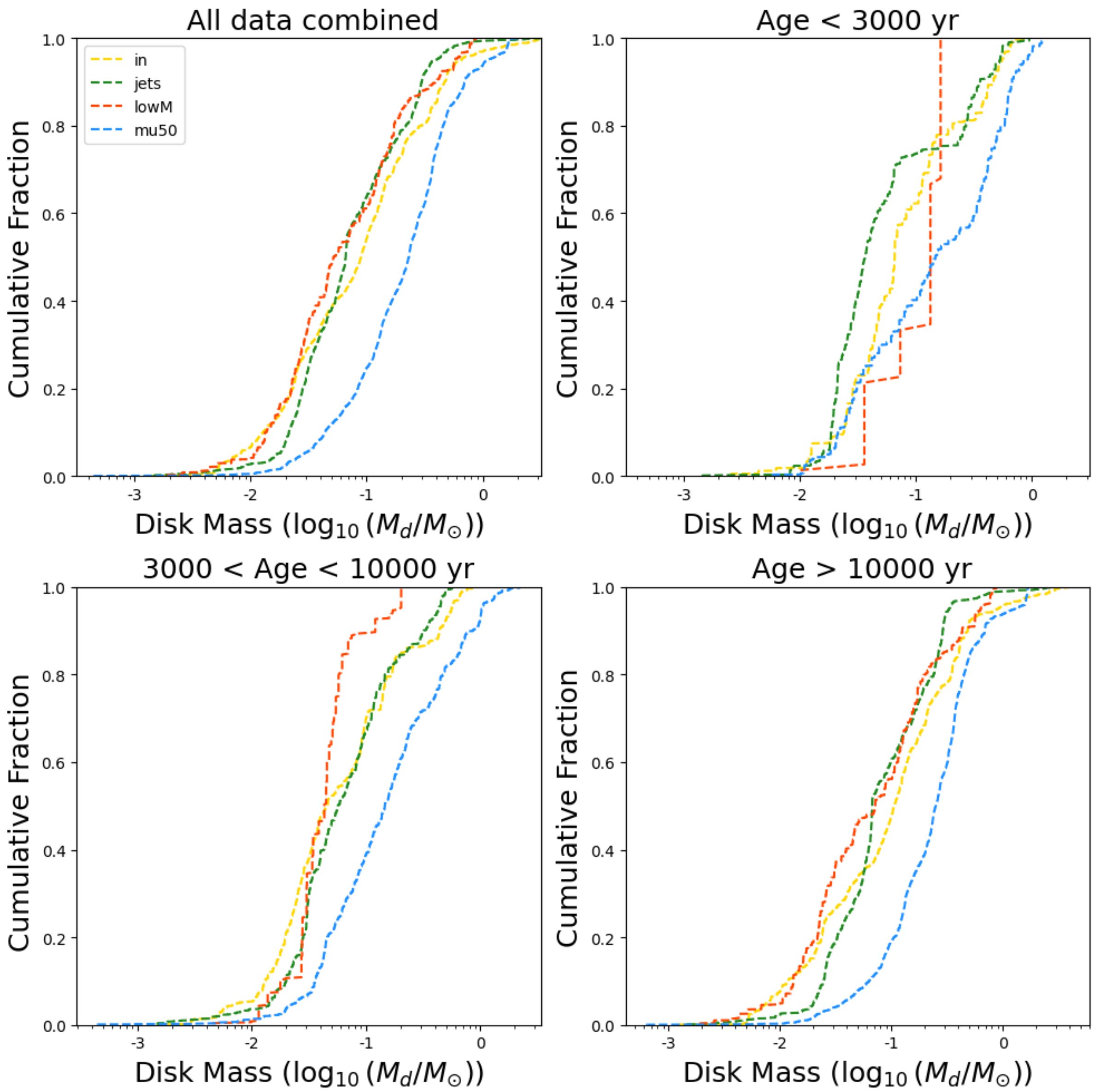

Figure 4.8: Age-dependent cumulative distribution of disk mass.

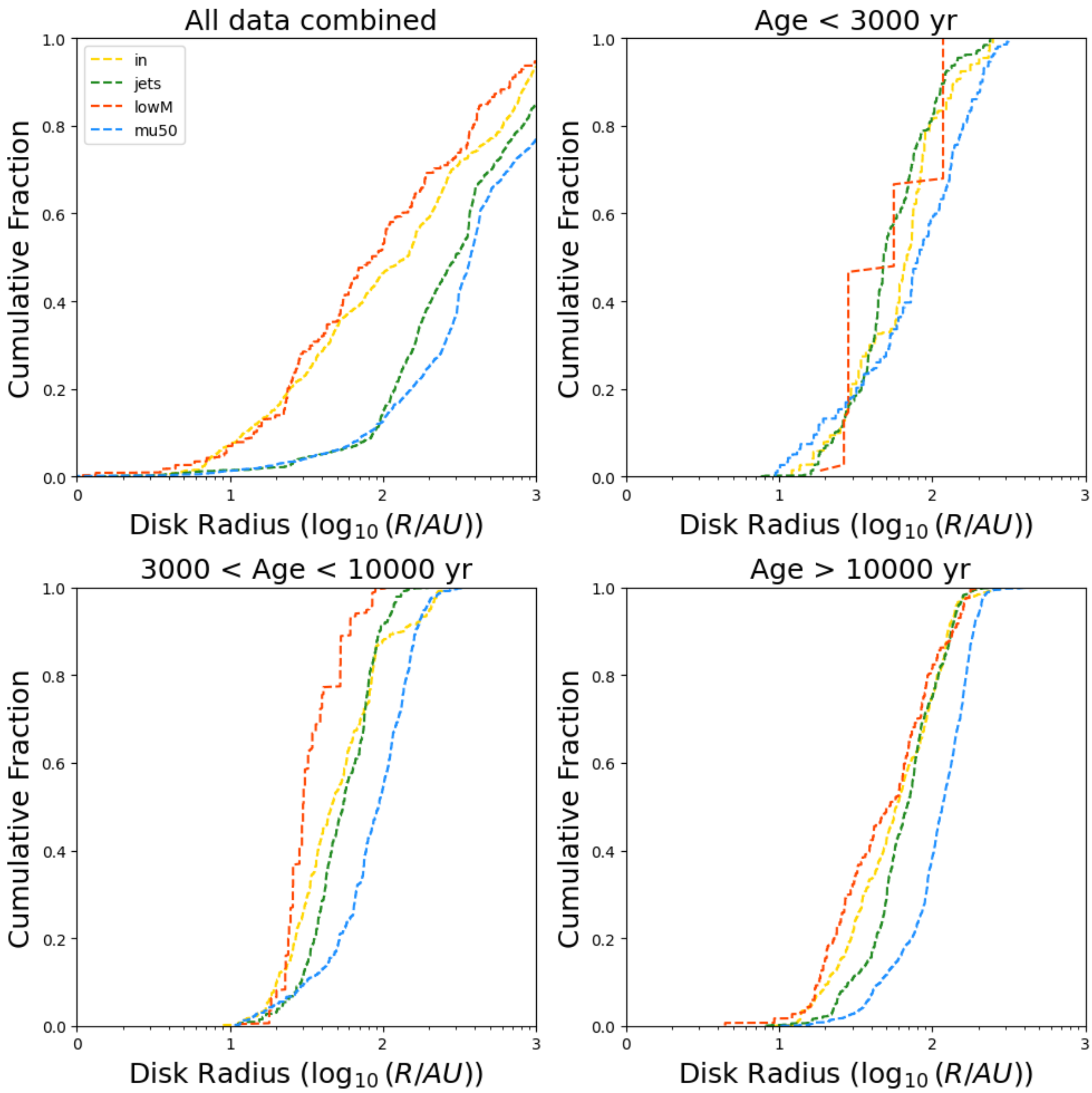

Figure 4.9: Age-dependent cumulative distribution of disk radius.

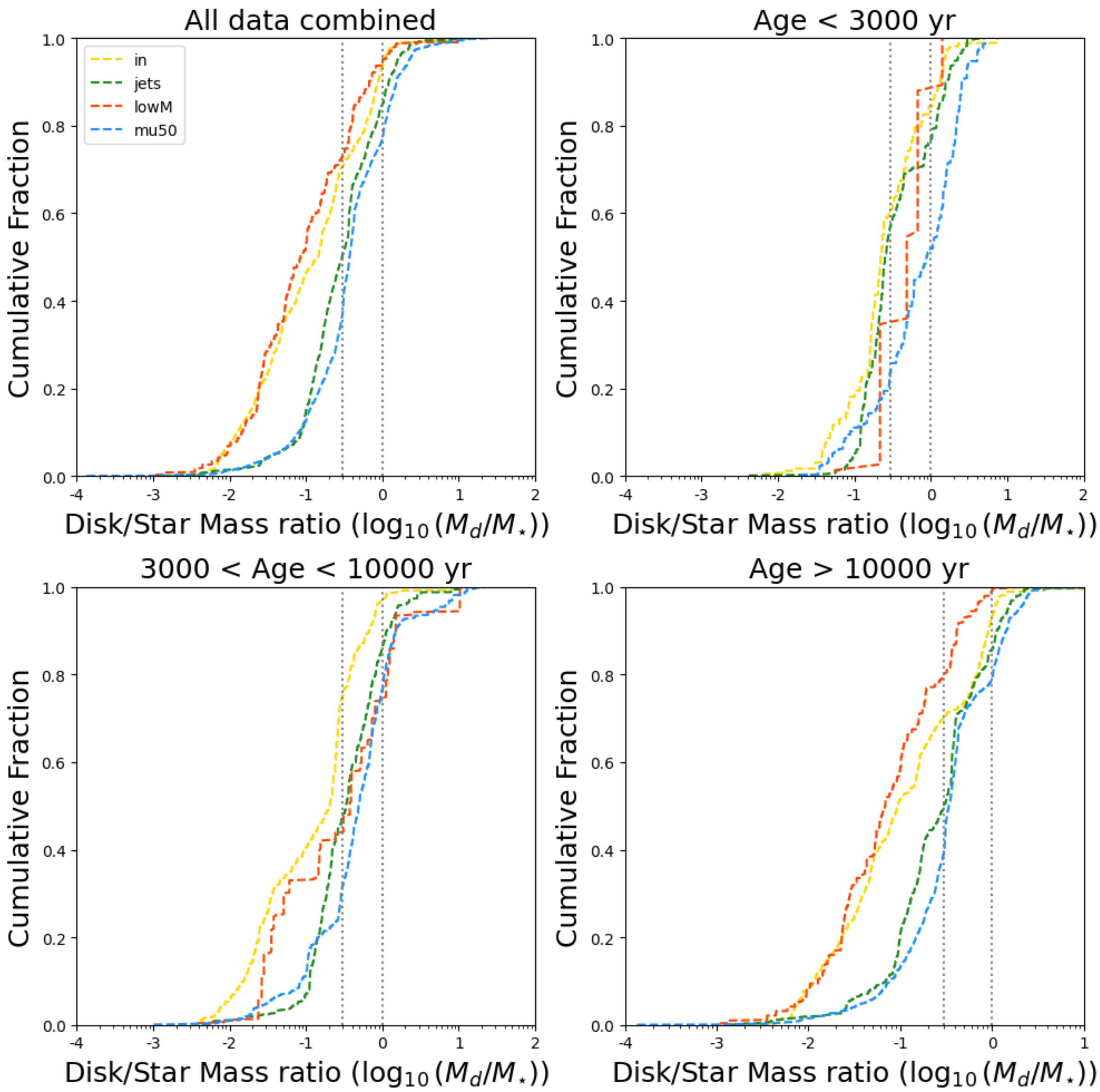

Figure 4.10: Age-dependent cumulative distribution of the disk-to-star mass ratio.

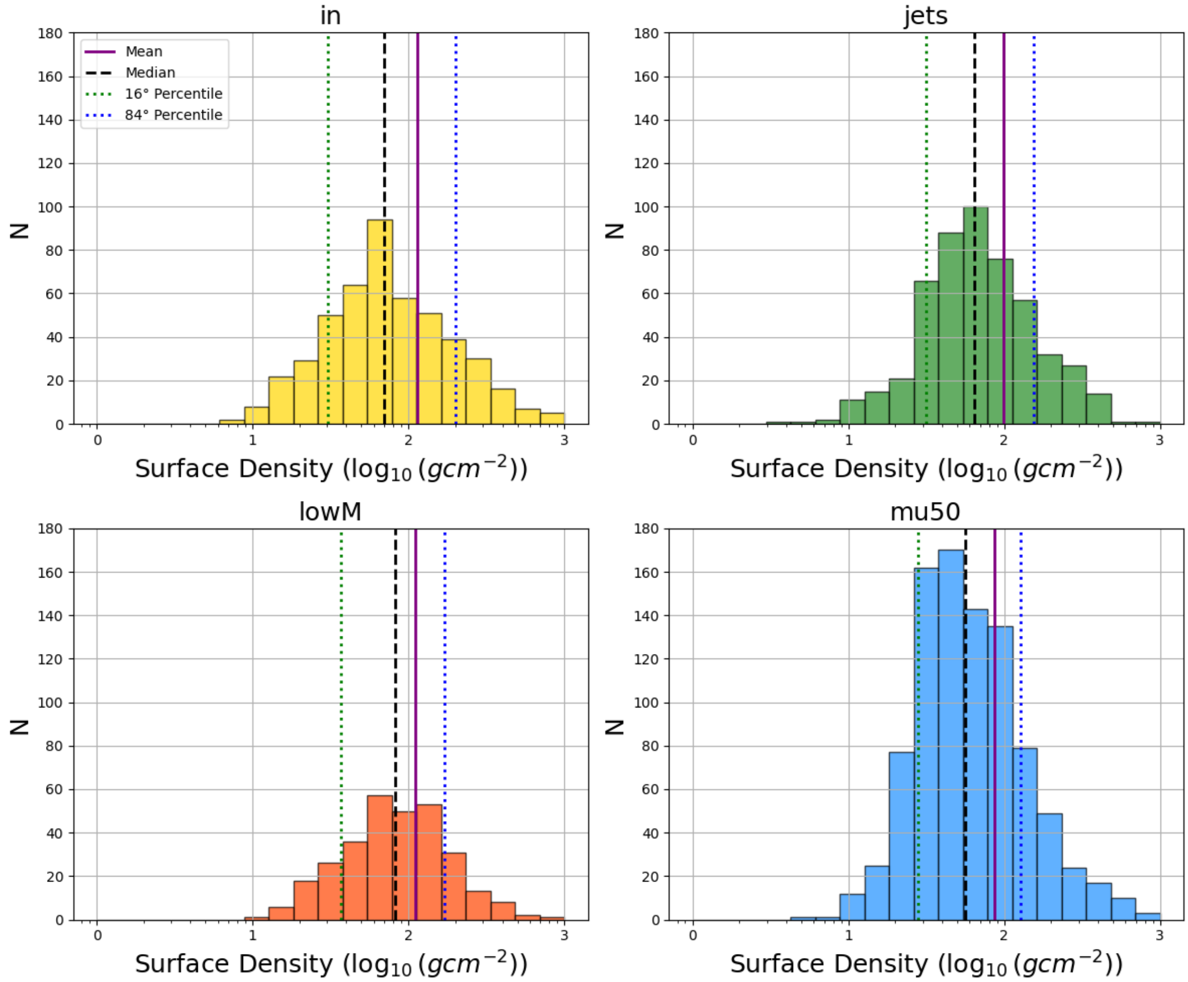

Figure 4.11: Cumulative distribution of the disk surface density for the four models, showing the mean, median and 16th and 84th percentile.

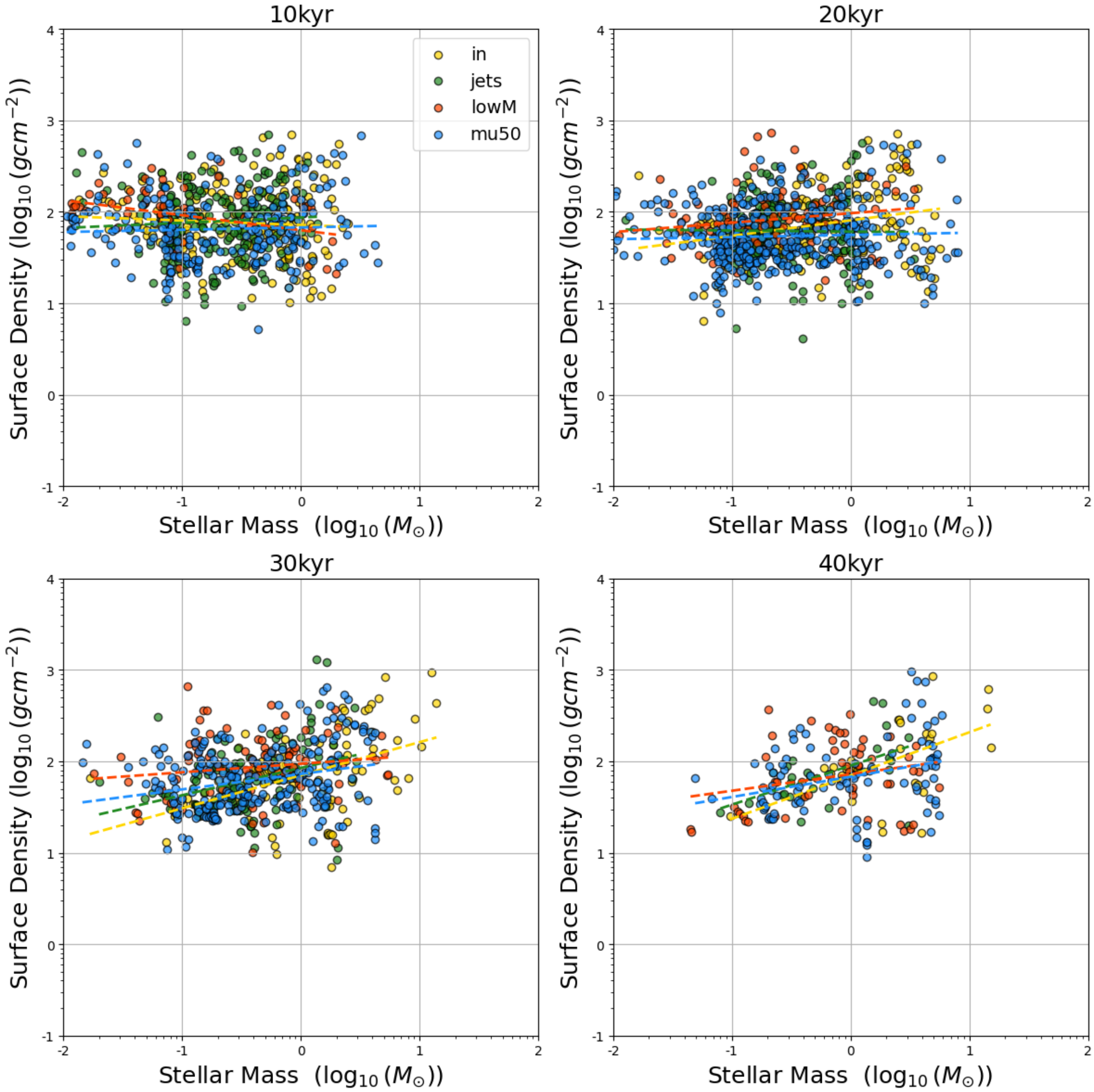

Figure 4.12: Surface density versus stellar mass at four different evolutionary times (10 kyr, 20 kyr, 30 kyr, 40 kyr). Each time panel includes data from all MHD models (in, jets, lowM, mu50).

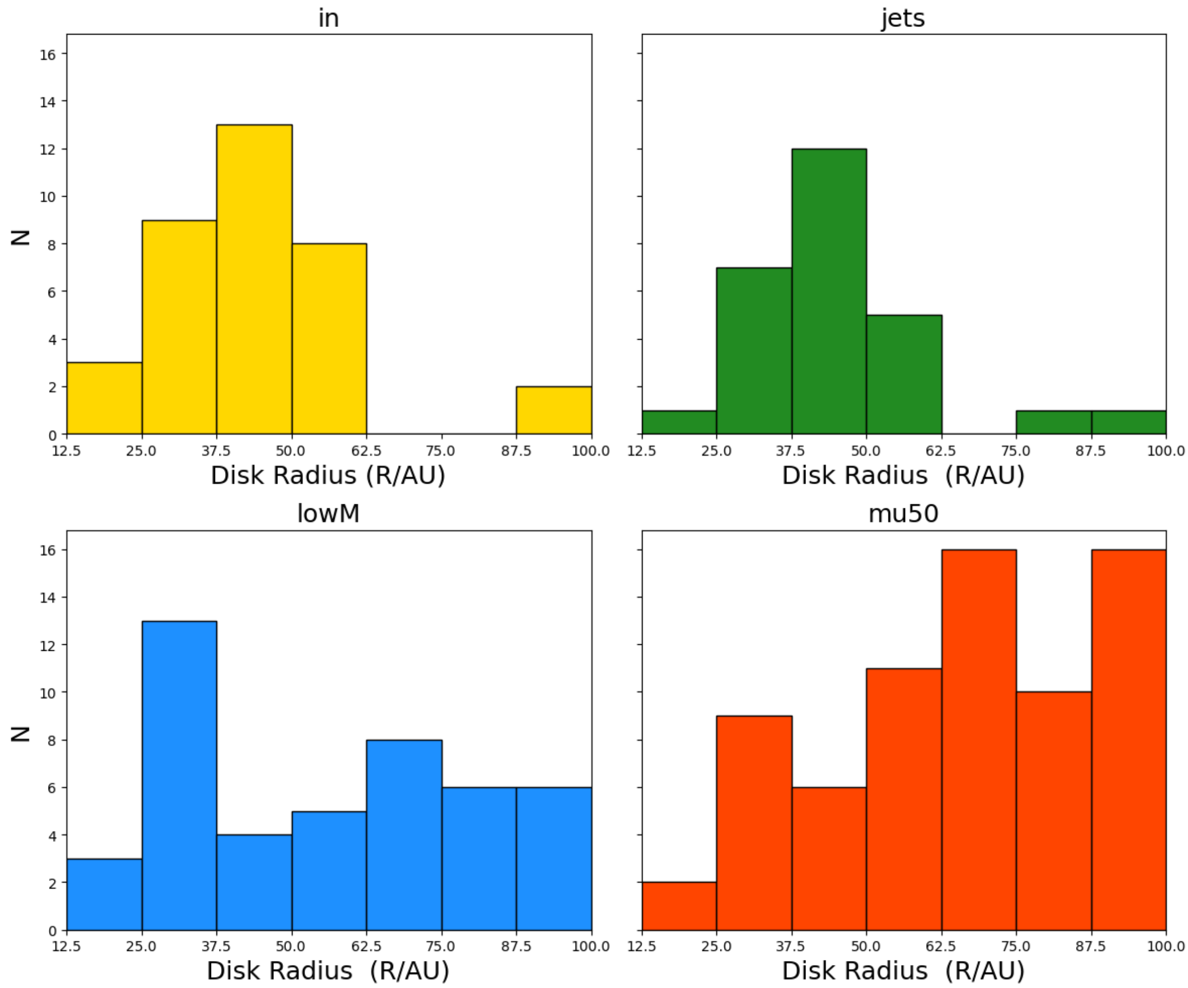

Figure 4.13: Histograms of disk radius for each model (in, jets, lowM, mu50), focusing on the brown dwarf population.

4.6 Exploring the Role of Beta parameter in Disk Radius, Stellar Mass, and Surface Density

Until now we analyze average simulation properties of the disks, this part will concentrate on specific properties of each disk, with a particular focus on the beta parameter related to the magnetic field. Previous studies have highlighted the importance of the magnetic field in this context, and the present study aims to provide a more detailed understanding of its role. In this analysis, the beta parameter was plotted as a function of disk radius for the four MHD models, considering both the aggregated dataset 4.14 and subsets divided by three stellar mass ranges 4.15, 4.16, 4.17, 4.18. For the aggregated data, a logarithmic fit was performed. The results confirm the expectations that larger disks tend to exhibit lower beta values. In this context, the beta parameter is defined as the ratio of gas pressure to magnetic pressure, with lower beta values indicating a greater dominance of magnetic forces relative to gas pressure. Another way to interpret the beta parameter is that it tells us the amount of magnetic field stored in the disc during its formation. This value also serves to predict the influence of the magnetic field on the disk's subsequent evolution, for instance, regulating the angular momentum distribution more effectively, which may allow the disk to extend further before being truncated. An examination of the plot of Beta versus Disk Radius reveals a discernible common trend between the models. Indeed, an increase in Beta is predicted to result in a decrease in Radius. This trend is consistent across various mass ranges, thereby reinforcing the conclusion that magnetic field dynamics play a critical role in determining the final Disk Radius. The beta versus stellar mass graph 4.19 further corroborates the hypothesis that stronger magnetic fields (i.e., lower beta values) are associated with larger and more massive systems. Specifically, it is observed that more massive stars are paired with lower beta values, indicating a relatively greater influence of magnetic pressure in these systems. Conversely, systems with lower stellar mass tend to exhibit higher beta values, where gas pressure dominates. This finding serves to reinforce our theoretical expectations regarding the interplay between magnetic fields and stellar mass, while also underscoring the pivotal role of magnetic dynamics in the evolution of disk and stellar properties. As illustrated in the final graph 4.20, the surface density is plotted as a function of beta for all four models and for three distinct stellar mass ranges. The trends observed across the different mass ranges closely mirror the overall behaviour seen in the aggregated data, with no significant deviations among the groups. This pattern is consistent with the findings of previous studies and confirms the hypothesis that systems characterized by higher beta values – indicative of a weaker magnetic field – exhibit higher surface densities, and vice versa. Another important thing to remember is that this happens even though we find disks with a lower radius in higher magnetic fields. These findings further emphasize the crucial role of magnetic field strength in influencing the disk surface density in star-forming systems.

4.7 Brown Dwarf Disk Characteristics and Implications

In summary, the analysis of the brown dwarf regime reveals distinct disk properties compared to those of higher-mass stars.The results demonstrate that the in and `jets` models tend to produce smaller disk radii for brown dwarfs, whereas both the `lowM` and `mu50` models yield larger disks. This similarity between `lowM` (with reduced initial clump mass) and `mu50` (characterized by a significantly weaker magnetic field) suggests that a decrease in either the mass or the magnetic field strength exerts comparable effects on the formation and final size of brown dwarf disks. These outcomes also imply that the magnetic field plays a pivotal role in regulating disk structure, as lower magnetic pressures (reflected by lower beta values) can facilitate the formation of more extended disks. In conclusion, the findings from the study of brown dwarfs underscore the significance of initial conditions and magnetic dynamics in modulating disk stability and evolution, thus offering pivotal insights into the process of substellar formation.

4.8 Summary

The findings underscore the necessity of quantifying not solely the disc radius and mass, but also the magnetic field, to impose more stringent constraints on the initial conditions of planetary formation. These measurements constitute a foundational element in comprehending the mechanisms that govern the formation of planetary systems, thereby diminishing the extensive range of parameters that exert influence during the embryonic phases. Moreover, it is imperative to increase the number of observations to enhance the statistical robustness, particularly in the context of brown dwarfs. To date, the majority of research in this area has been conducted in nearby star-forming regions. However, in order to obtain a more comprehensive and representative understanding of their evolution, it is necessary to extend these investigations to other regions.

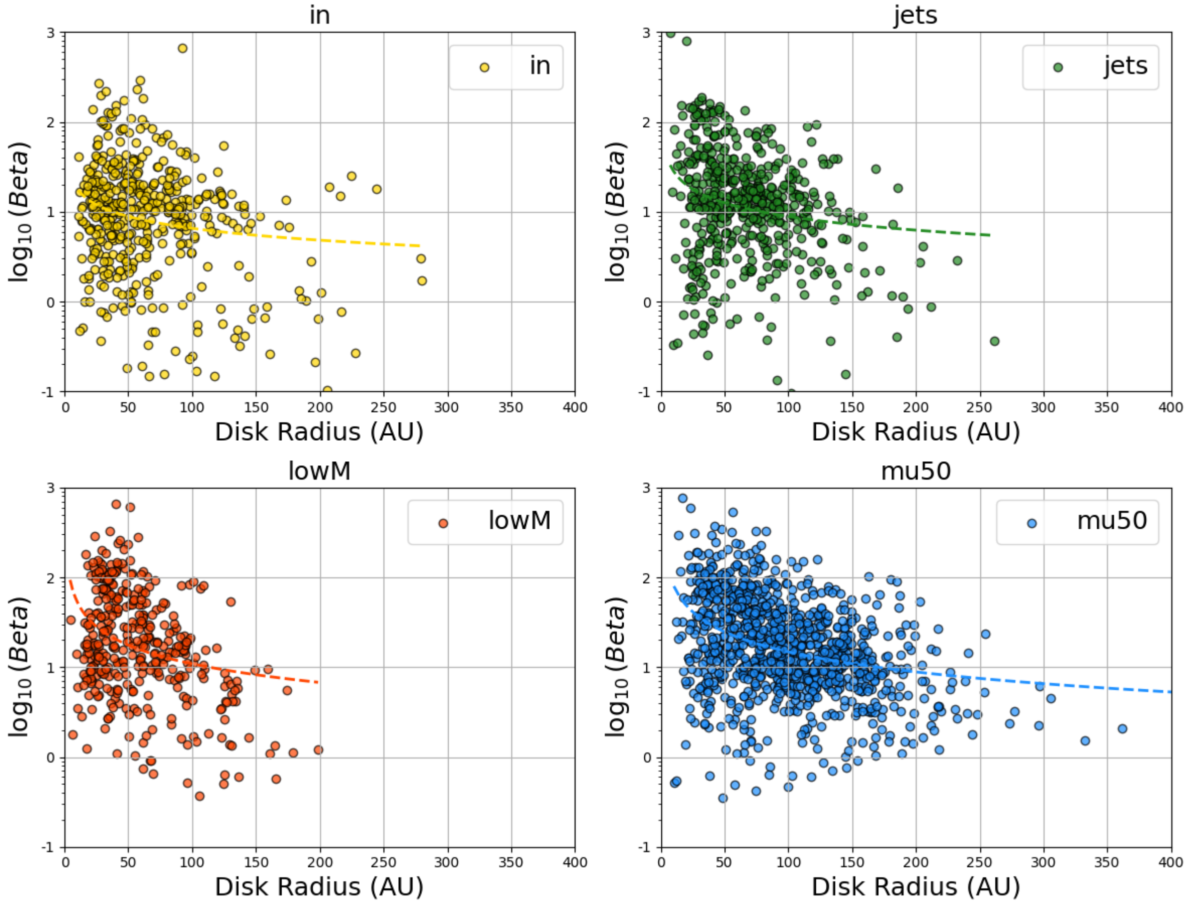

Figure 4.14: Scatter plot for the four models for the Beta parameter in function of the disk radius and their rispective logarithmic fit.

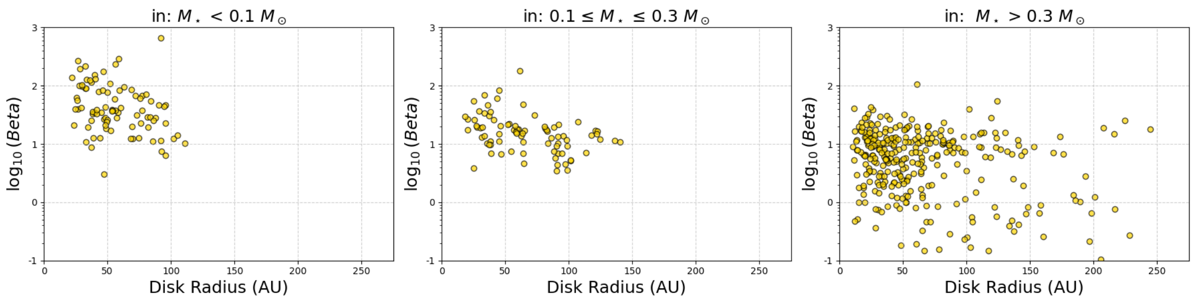

Figure 4.15: Scatter plot for the Beta parameter in 3 different mass regimes in function of the disk radius for the model in.

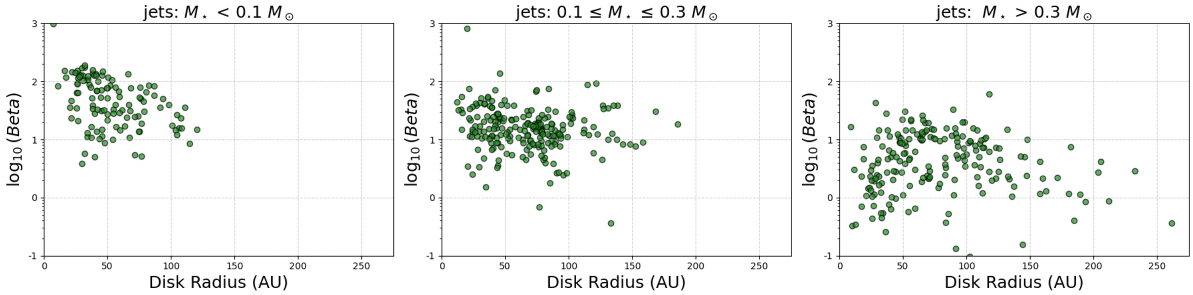

Figure 4.16: Scatter plot for the Beta parameter in 3 different mass regimes in function of the disk radius for the model jets.

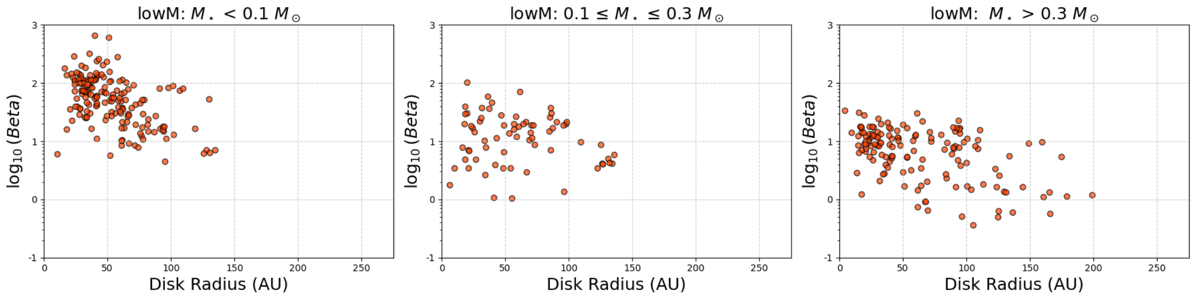

Figure 4.17: Scatter plot for the Beta parameter in 3 different mass regimes in function of the disk radius for the model lowM.

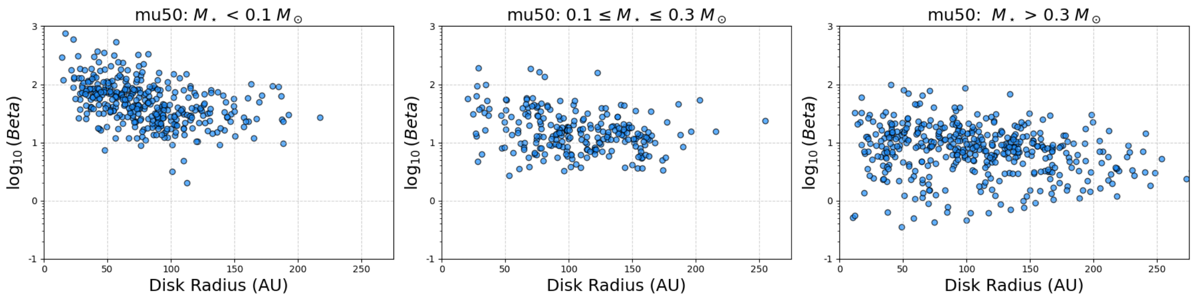

Figure 4.18: Scatter plot for the Beta parameter in 3 different mass regimes in function of the disk radius for the model mu50.

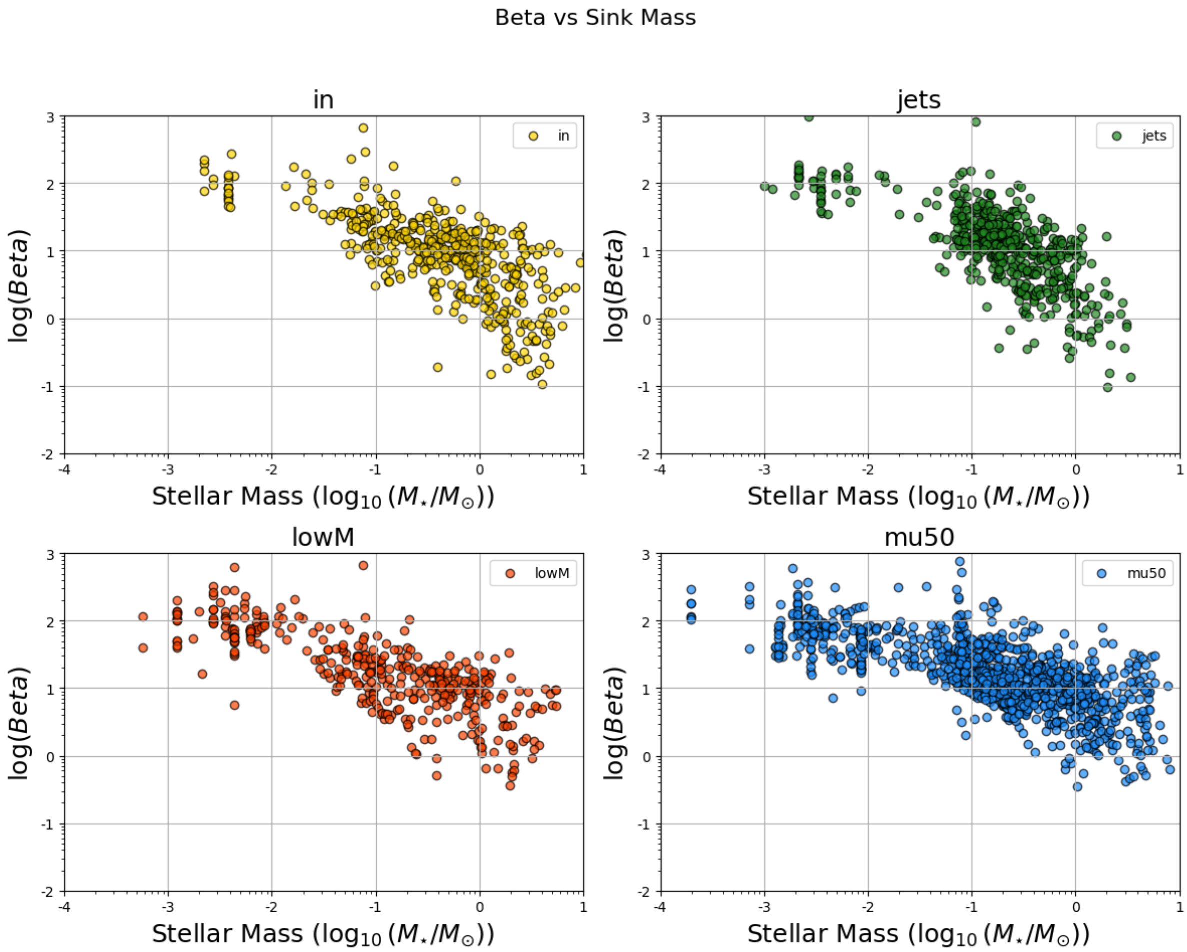

Figure 4.19: Scatter plot for the Beta parameter as a function of the stellar mass for the four models.

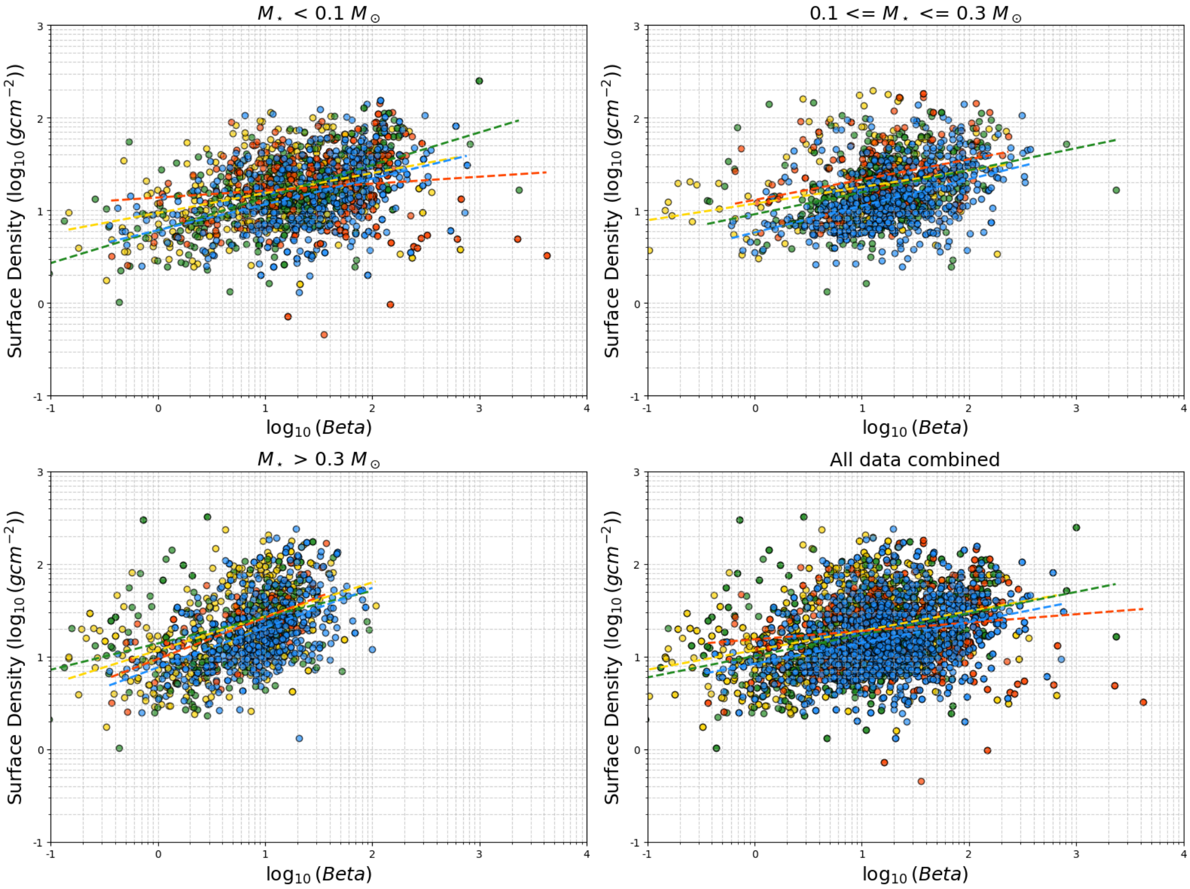

Figure 4.20: Disk surface density versus Beta, shown for three different stellar mass bins and for all data combined, with their respectivem logarithmic fits.

Chapter 5

Conclusions

This thesis provides an in-depth comparative analysis of classical simulation models based on Bate's SPH methodology and a new generation of models that integrate magneto-hydrodynamic (MHD) effects, such as ambipolar diffusion, alongside radiative feedback and, in some cases, protostellar jets. The obtained results demonstrate that the incorporation of magnetic fields and related physical processes significantly alters the angular momentum transport and fragmentation regime during the collapse of molecular cores. In particular, the MHD models have a tendency to suppress excessive fragmentation, resulting in disk properties that differ substantially from those predicted by the classical models. As far as the IMF is concerned, it's in good agreement with the classical models, even if the total number of stars is very different. The analysis of cumulative stellar mass distributions, accretion rates, and disk characteristics reveals that the presence of magnetic fields, in combination with radiative feedback and jet effects, leads to disks that are less massive yet structurally distinct, influencing the overall efficiency of mass transport and the temporal evolution of protoplanetary systems. Furthermore, the study has investigated various relationships associated with the beta parameter, thereby shedding light on its role in mediating the effects of the magnetic field on disk radius, stellar mass, and surface density distributions. This further enhances our understanding of how magnetic field strength and configuration impact star and disk formation. Looking ahead, several future research directions are identified to further enhance our understanding:

- **Disk Dimensions Analysis**: A more detailed study of the dimensions of the disks is important to better determine their properties. This will be possible thanks to the ALMA telescope [61].
- **Longer Wavelength Post Processing of Simulations**: It is crucial to perform synthetic observations at longer wavelengths to assess whether the SKA telescope can assist in accurately measuring disk masses, an observable that is notably challenging to determine.

- **Accretion Rate Discrepancies**:A significant difference in accretion rates is observed between protostars and pre-main sequence stars, with the possible exception of the `jets` model. Therefore, it will be important to investigate the relationship between the accretion rate and stellar mass during the final stages of star formation, prior to the disk transitioning to the Class II stage of YSOs [26].

- **Magnetic Field Measurements**: Despite the inherent difficulties in measuring magnetic fields, initiatives such as the large ENYGMA programme for IRAM/NOEMA have been developed to better understand their influence on disk formation. Continued efforts in this area are essential.

- **Tracer Particles in Simulations**: Implementing tracer particles in future simulations will allow for a more detailed study of the inflow from the clump and circulation within the disk. This is particularly important for understanding the initial conditions of planet formation, especially in determining the disk's surface density.

Overall, these findings not only emphasize the importance of incorporating magnetic and feedback processes in star and disk formation simulations but also offer new insights for more accurate comparisons between simulation predictions and observational data. Ultimately, this work contributes to a deeper understanding of the mechanisms governing the formation of brown dwarfs and their disks, outlining the physical conditions necessary for the development of environments conducive to planet formation in low-mass regimes.

Chapter 6

Appendix

In this appendix, a series of plots is presented which illustrate the evolution of disk properties across different mass ranges and time snapshots. The initial four figures 6.1, 6.2, 6.3, 6.4 show histograms of the surface density at 10 kyr, 20 kyr, 30 kyr, and 40 kyr, divided into three mass bins. Each panel in the series provides a visual representation of the alterations in the distribution of surface density over time for a specific mass range. These alterations are further delineated by the presence of vertical lines, which demarcate key statistical markers such as the mean and median values, in addition to the 16th and 84th percentiles. The final figure 6.5 presents scatter plots of temperature versus disk radius for the same time frames and mass bins. These plots facilitate the illustration of the relationship between disk size and thermal properties, as well as the manner in which this relationship is contingent on the mass range and evolutionary stage. In summary, these figures provide a comprehensive overview of the evolution of disk structure and temperature over time for low-mass protostellar objects under different conditions.

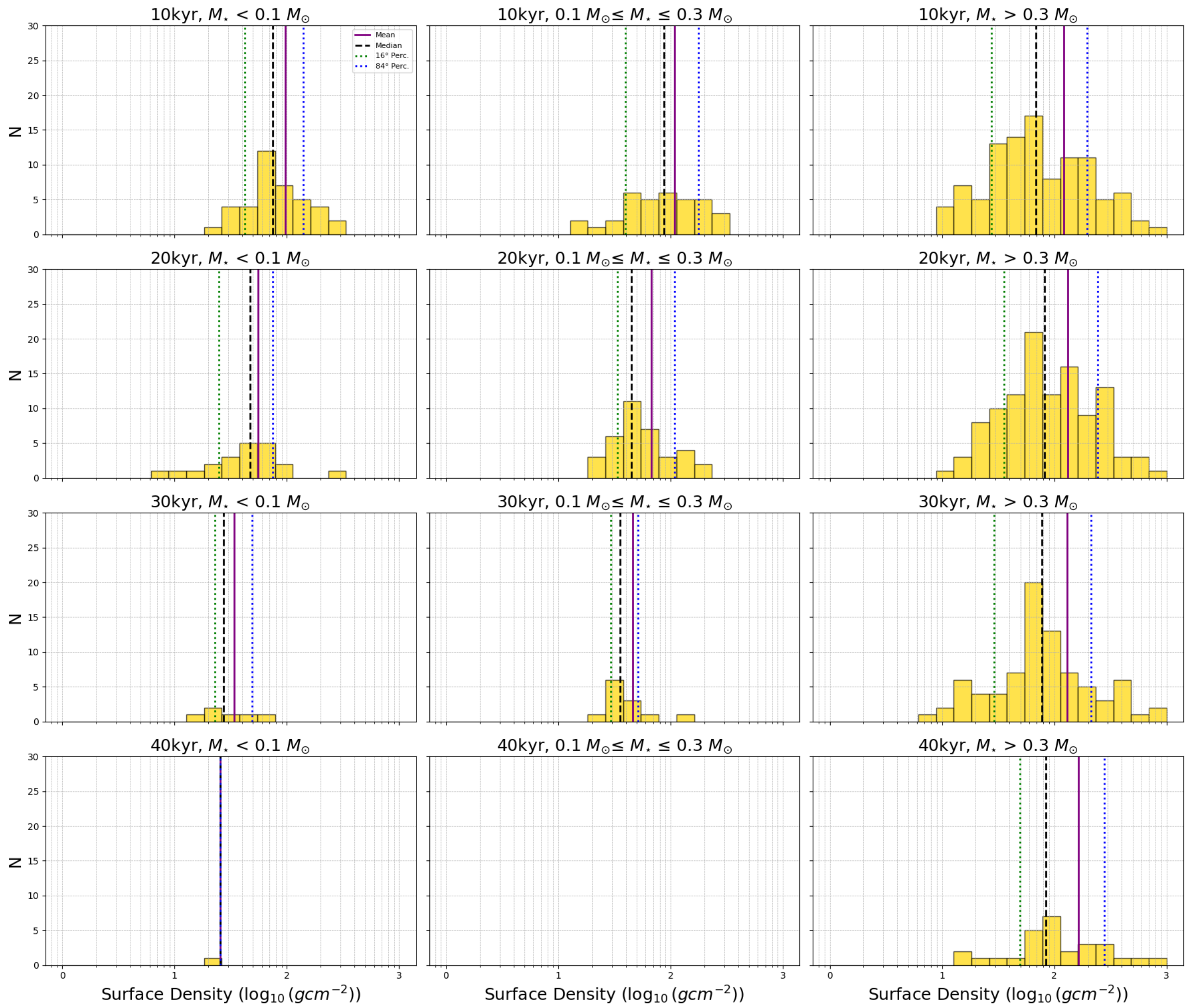

Figure 6.1: Disk surface density profile for the "in" model, showing the mean, median and 16th and 84th percentile.

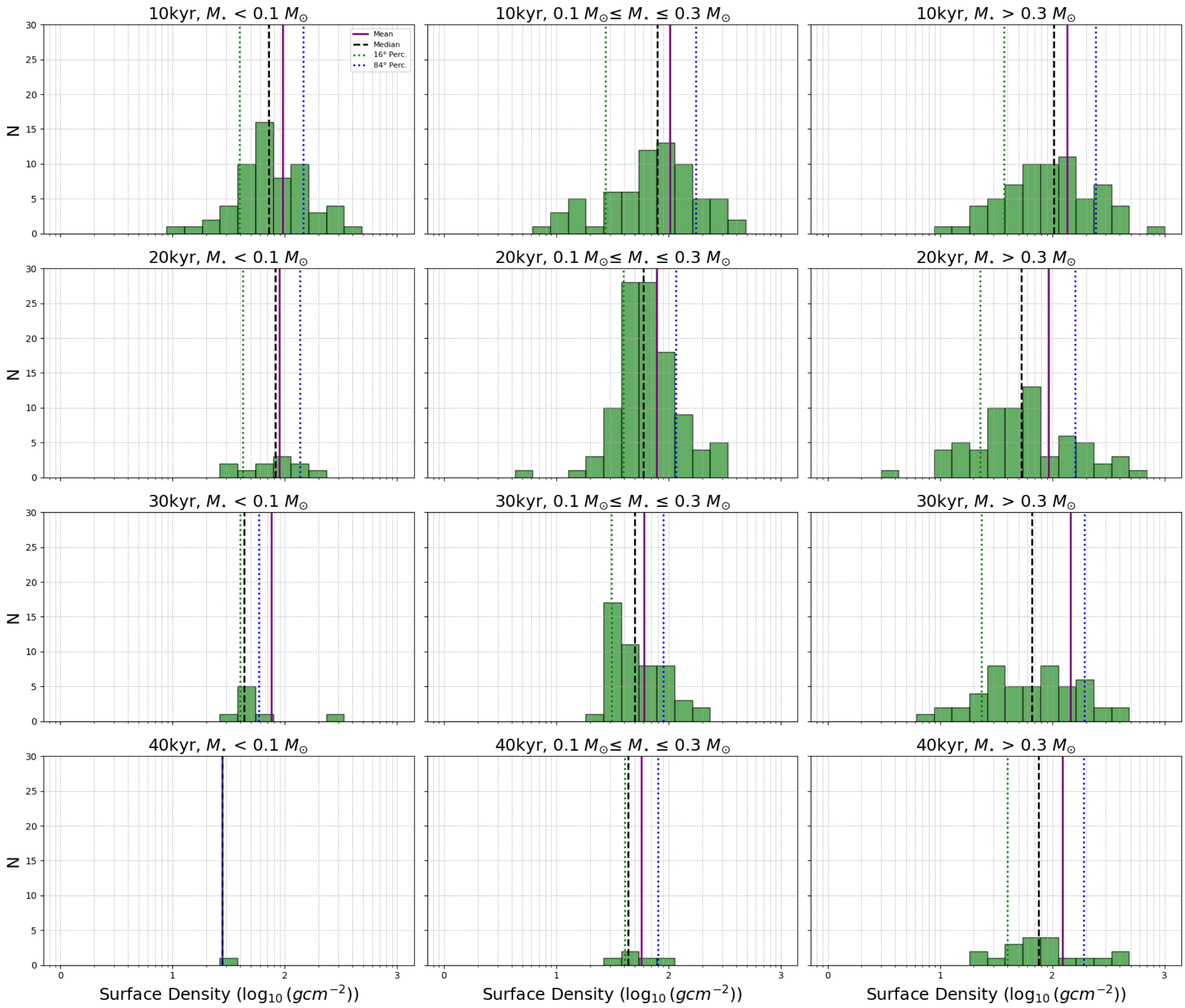

Figure 6.2: Disk surface density profile for the "jets" model, showing the mean, median and 16th and 84th percentile.

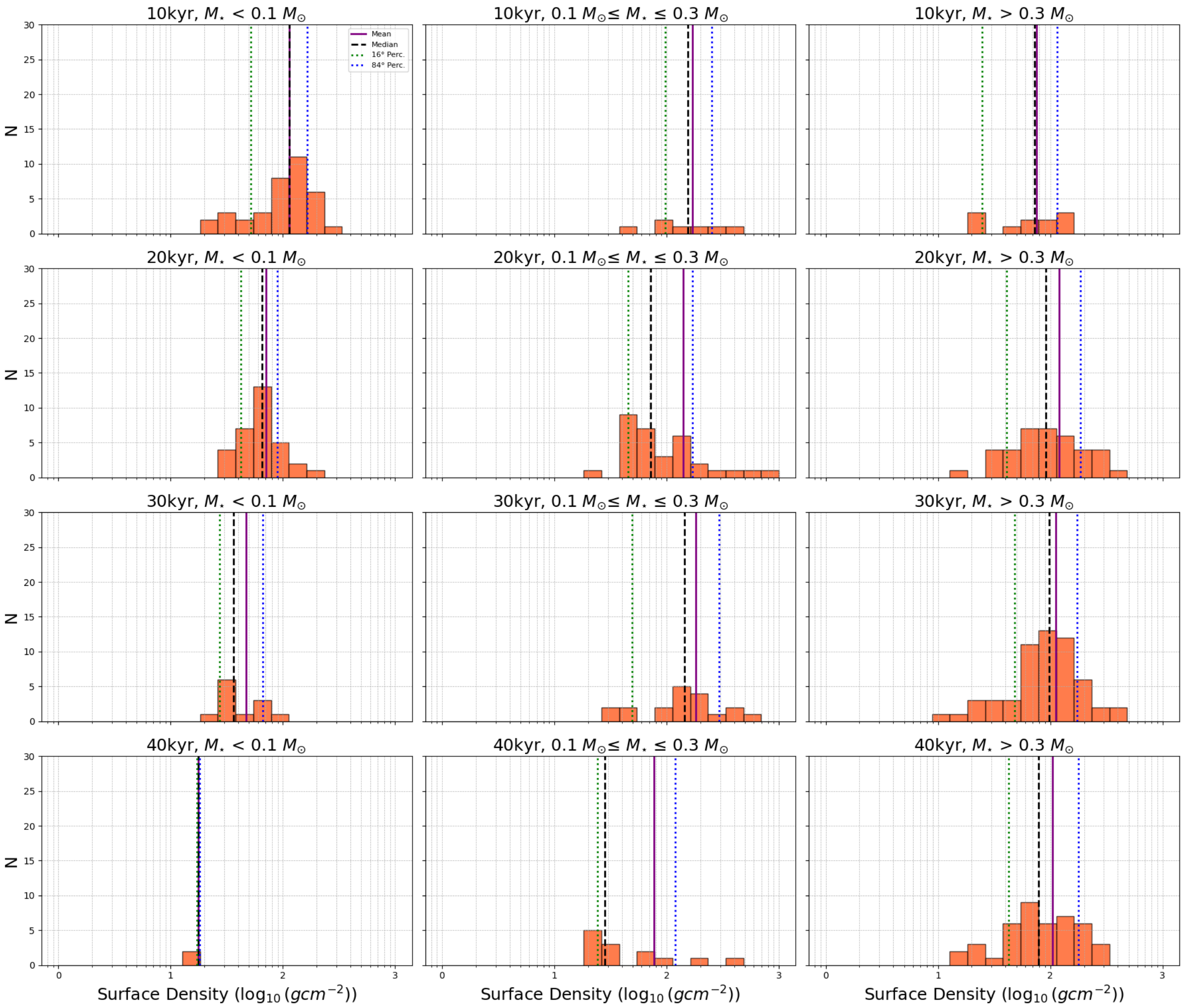

Figure 6.3: Disk surface density profile for the "lowM" model, showing the mean, median and 16th and 84th percentile.

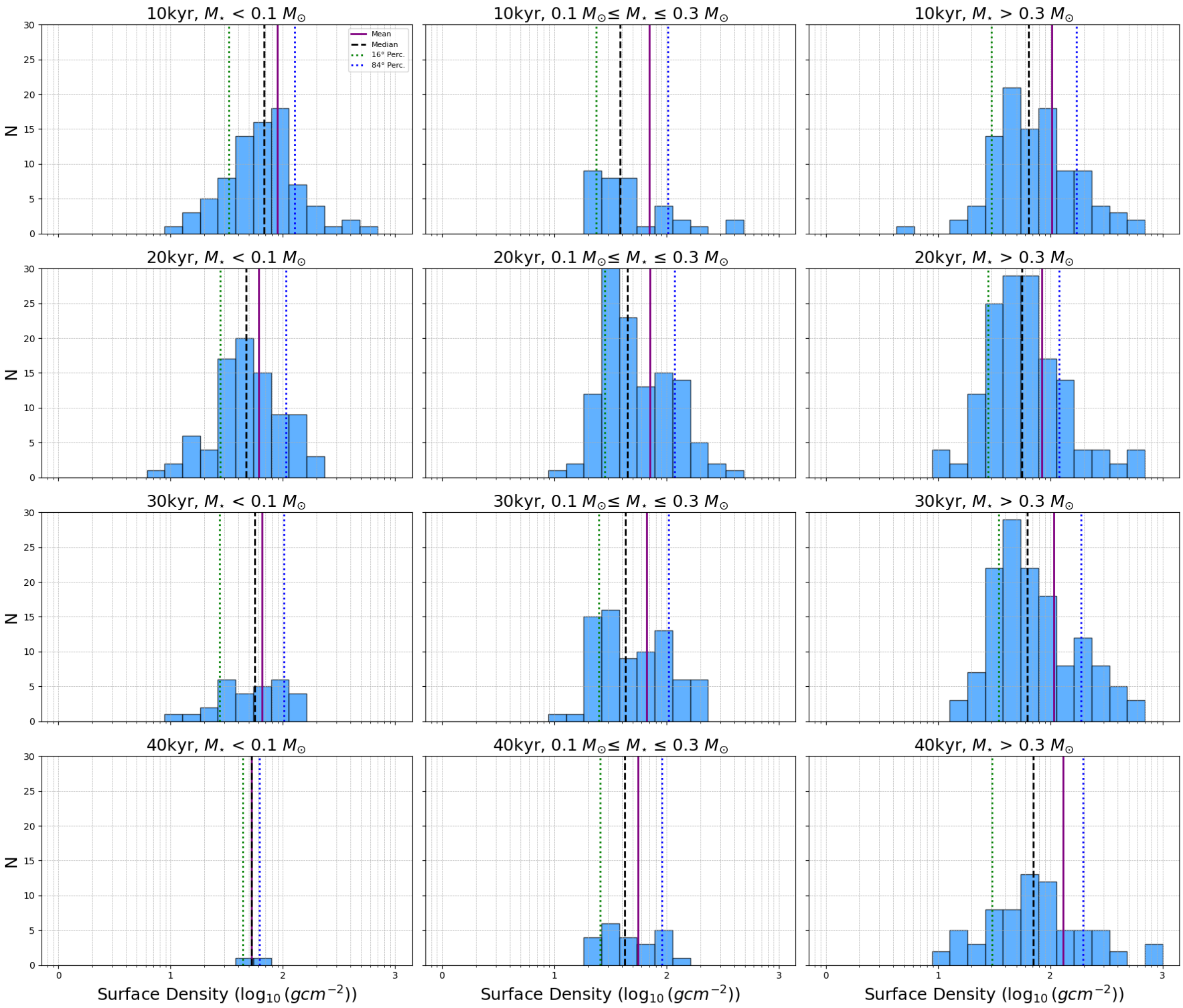

Figure 6.4: Disk surface density profile for the "mu50" model, showing the mean, median and 16th and 84th percentile.

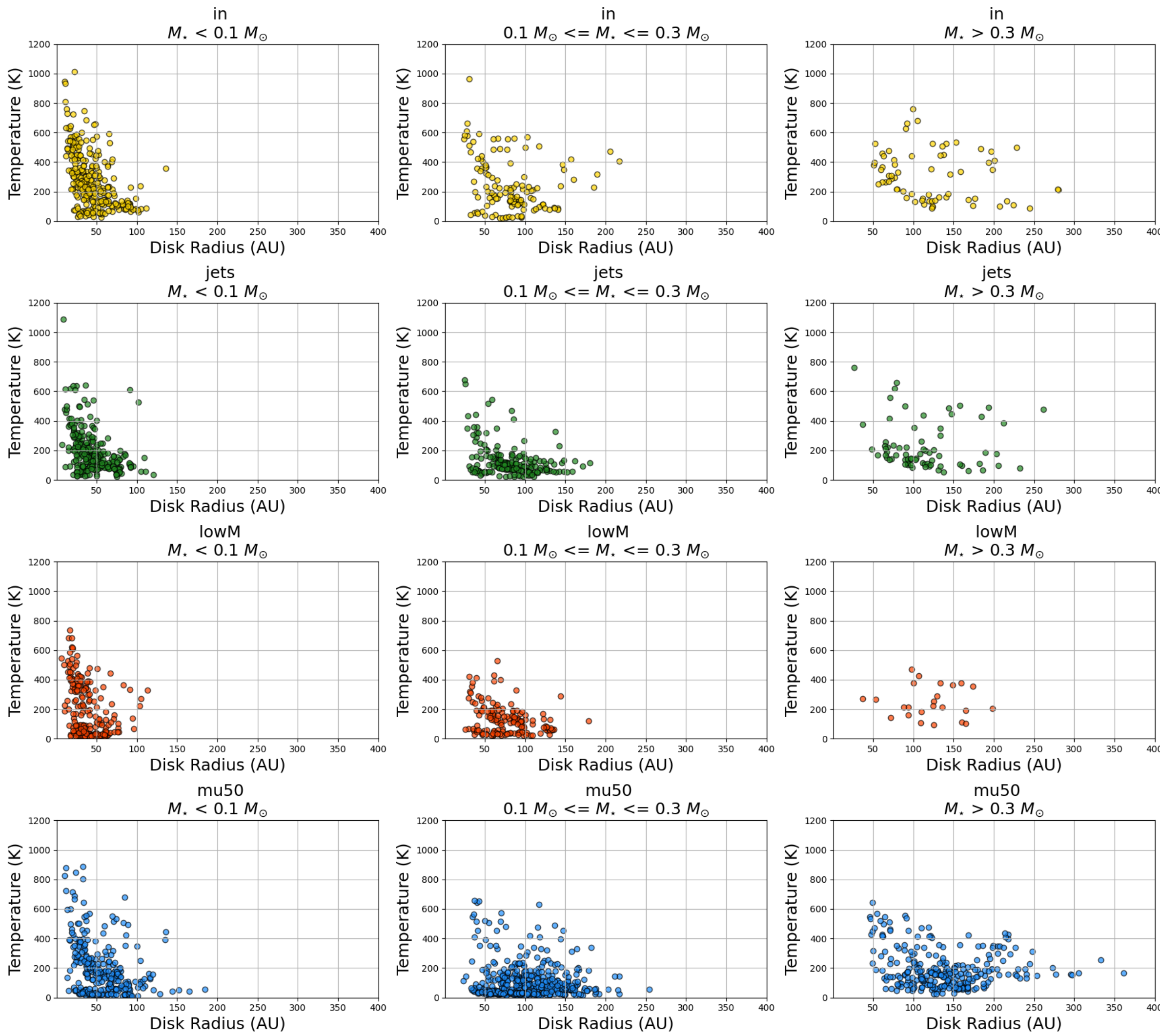

Figure 6.5: Disk temperature as a function of disk radius, separated into three stellar mass bins for each MHD model.

Bibliography

[1] https://www.esa.int/Science_Exploration/Space_Science/Born_in_beauty_proplyds_in_the_Orion_Nebula.

[2] https://www.nasa.gov/universe/nasas-webb-findings-support-long-proposed-process-of-planet-formation.

[3] C. et al. . Jwst detects neon line variability in a protoplanetary disk. *The Astrophysical Journal Letters, Volume 958, Number 1*, 2023.

[4] Pascucci I. Andrews S. Armitage P. Cieza L. Alexander, R. *Protostars and Planets VI.* 2014.

[5] S. M. Andrews. The disk substructures at high angular resolution project (dsharp). i. motivation, sample, calibration, and overview. *The Astrophysical Journal Letters, Volume 869, Number 2*, 2018.

[6] S.M. et al. Andrews. Protoplanetary disk structures in ophiuchus. *The Astrophysical Journal, Volume 700, Issue 2, pp. 1502-1523 (2009)*, 2009.

[7] P. J. Armitage. Physical processes in protoplanetary disks. *"From Protoplanetary Disks to Planet Formation"*, 2017.

[8] S. A. Balbus and J. F. Hawley. A powerful local shear instability in weakly magnetized disks. i. linear analysis. *Astrophysical Journal v.376, p.214*, 1991.

[9] J. Barnes and P. Hut. A hierarchical o(n log n) force-calculation algorithm. *Nature, Volume 324, pages 446–449*, 1986.

[10] Bonnell I. A. Bate, M. R. and N. M. Price. Modelling accretion in protobinary systems. *Monthly Notices of the Royal Astronomical Society, Volume 277, Issue 2, November 1995, Pages 362–376*, 1995.

[11] M. R. Bate. Stellar, brown dwarf, and multiple star properties from hydrodynamical simulations of star cluster formation. *Monthly Notices of the Royal Astronomical Society, Volume 392, Issue 2, pp. 590-616*, 2008.

[12] M. R. Bate. Stellar, brown dwarf, and multiple star properties from hydrodynamical simulations of star cluster formation. *Monthly Notices of the Royal Astronomical Society, Volume 418, Issue 1, pp. 703-704*, 2011.

[13] M. R. Bate. On the diversity and statistical properties of protostellar discs. *Monthly Notices of the Royal Astronomical Society, Volume 475, Issue 4, April 2018, Pages 5618–5658*, 2018.

[14] W. Benz. Smooth particle hydrodynamics: A review. *The Numerical Modelling of Nonlinear Stellar Pulsatations*, 1990.

[15] R.D. Blendford and G.D. Payne. Hydromagnetic flows from accretion discs and the production of radio jets. *Monthly Notices of the Royal Astronomical Society, Vol. 199, 883-903*, 1982.

[16] J. Blum and G. Wurm. The growth mechanisms of macroscopic bodies in protoplanetary disks. *Annual Review of Astronomy and Astrophysics, Vol. 46:21-56*, 2008.

[17] S. et al. Chatterjee. Dynamical outcomes of planet-planet scattering. *The Astrophysical Journal, Volume 686, Number 1*, 2008.

[18] M. et al. Chevance. The life and times of giant molecular clouds. *Protostars and Planets VII*, 2023.

[19] R. M. Crutcher. Magnetic fields in molecular clouds. *Annual Review of Astronomy and Astrophysics, vol. 50, p.29-63*, 2012.

[20] T.M. et al. Dame. The milky way in molecular clouds: A new complete co survey. *The Astrophysical Journal, Volume 547, Number 2*, 2001.

[21] G. et al. De Marchi. Protoplanetary discs around sun-like stars appear to live longer when the metallicity is low. *The Astrophysical Journal, Volume 977, Number 2*, 2024.

[22] C. P. et al. Dullemond. Models of the structure and evolution of protoplanetary disks. *Protostars and Planets V*, 2006.

[23] C. et al. Espaillat. An observational perspective of transitional disks. *Protostars and Planets VI*, 2014.

[24] N .J. II et al. Evans. The spitzer c2d legacy results: Star-formation rates and efficiencies; evolution and lifetimes. *The Astrophysical Journal Supplement, Volume 181, Issue 2, pp. 321-350*, 2009.

[25] K. M. Ferrière. The interstellar environment of our galaxy. *Reviews of Modern Physics 73:1031-1066,2001*, 2001.

[26] E. et al. Fiorellino. The mass accretion rate and stellar properties in class i protostars. *The Astrophysical Journal, 944:135 (21pp), 2023 February 20*, 2023.

[27] A. et al. Frank. Jets and outflows from star to cloud: Observations confront theory. *Protostars and Planets VI*, 2014.

[28] C. F. Gammie. Nonlinear outcome of gravitational instability in cooling, gaseous disks. *The Astrophysical Journal, Volume 553, Issue 1, pp. 174-183*, 2001.

[29] A. et al. Garufi. Three years of sphere: the latest view of the morphology and evolution of protoplanetary discs. *The Messenger, vol. 169, p. 32-37*, 2017.

[30] U. et al. Gorti. Disk dispersal: Theoretical understanding and observational constraints. *Space Science Reviews, Volume 205, Issue 1-4, pp. 125-152*, 2015.

[31] K. E. Jr. et al. Haisch. Disk frequencies and lifetimes in young clusters. *The Astrophysical Journal, Volume 553, Issue 2, pp. L153-L156*, 2001.

[32] L. et al. Hartmann. Accretion and the evolution of t tauri disks. *The Astrophysical Journal, Volume 495, Number 1*, 1998.

[33] Y. et al. Hasegawa. Determining dispersal mechanisms of protoplanetary disks using accretion and wind mass loss rates. *Astrophysical Journal Letters, Volume 926, Number 2*, 2025.

[34] C. Hayashi and T. Nakano. Evolution of stars of small masses in the pre-main-sequence stages. *Progress of Theoretical Physics, Volume 30, Issue 4, October 1963, Pages 460–474*, 1963.

[35] P. et al. Hennebelle. Magnetically self-regulated formation of early protoplanetary disks. *The Astrophysical Journal Letters, Volume 830, Number 1*, 2016.

[36] M.R. Hogerheijde. *Protoplanetary Disk*. Springer, 2011.

[37] A. Johansen and H. Klahr. Dust diffusion in protoplanetary disks by magnetorotational turbulence. *The Astrophysical Journal, Volume 634, Number 2*, 2005.

[38] A. Johansen and M. Lambrechts. Forming planets via pebble accretion. *Annual Review of Earth and Planetary Sciences, Vol. 45:359-387*, 2017.

[39] M.R. Krumholz and C. F. McKee. A general theory of turbulence-regulated star formation, from spirals to ultraluminous infrared galaxies. *The Astrophysical Journal, Volume 630, Issue 1, pp. 250-268.*, 2005.

[40] S.S. Kumar. The structure of stars of very low mass. *Astrophysical Journal, vol. 137, p.1121*, 1963.

[41] C. J. Lada and B.A. Wilking. The nature of the embedded population in the rho ophiuchi dark cloud - mid-infrared observations. *Astrophysical Journal, Vol. 287, p. 610-621*, 1984.

[42] U. et al. Lebreuilly. Synthetic populations of protoplanetary disks. impact of magnetic fields and radiative transfer. *Astronomy Astrophysics*, 2023.

[43] G. et al. Lesur. Hydro-, magnetohydro-, and dust-gas dynamics of protoplanetary disks. *Protostars and Planets VII*, 2022.

[44] M.-M. Mac Low and R. S. Klessen. *Control of star formation by supersonic turbulence*, volume 76. Reviews of Modern Physics, 2004.

[45] M. Mayor and D. Queloz. A jupiter-mass companion to a solar-type star. *Nature, Volume 378, Issue 6555, pp. 355-359*, 1995.

[46] J. J. Monaghan. Smoothed particle hydrodynamics. *Annual Review of Astronomy and Astrophysics, Vol. 30, p. 543-574*, 1992.

[47] T. Ch. Mouschovias and Jr. Spitzer, L. Note on the collapse of magnetic interstellar clouds. *Astrophysical Journal, vol. 210, Dec. 1, 1976, pt. 1, p. 326, 327.*, 1976.

[48] K. I. et al. Oberg. The spitzer ice legacy: ice evolution from cores to protostars. *The Astrophysical Journal, Volume 740, Issue 2, article id. 109, 16 pp.*, 2011.

[49] C. W. Ormel and H. H. Klhar. The effect of gas drag on the growth of protoplanets. analytical expressions for the accretion of small bodies in laminar disks. *Astronomy and Astrophysics, Volume 520, September-October 2010*, 2010.

[50] P. et al. Padoan. The star formation rate of molecular clouds. *Protostars and Planets VI*, 2014.

[51] T. et al. Paneque-Carreño. Spiral arms and a massive dust disk with non-keplerian kinematics: Possible evidence for gravitational instability in the disk of elias 2–27. *The Astrophysical Journal, Volume 914, Number 2*, 2021.

[52] I. Rabago and Z. Zhaohuan. Constraining protoplanetary disk accretion and young planets using alma kinematic observations. *Monthly Notices of the Royal Astronomical Society, Volume 502, Issue 4, April 2021, Pages 5325–5339*, 2021.

[53] A. Riols and H. Latter. Spiral density waves and vertical circulation in protoplanetary discs. *Monthly Notices of the Royal Astronomical Society, Volume 476, Issue 4, June 2018, Pages 5115–5126*, 2018.

[54] P. J. et al. Rodenkirch. Modeling the nonaxisymmetric structure in the hd 163296 disk with planet-disk interaction. *Astronomy Astrophysics, Volume 647, id.A174, 18 pp.*, 2020.

[55] F. H. et al. Shu. Star formation in molecular clouds - observation and theory. *Annual review of astronomy and astrophysics, Vol. 25, p. 23-81*, 1987.

[56] L. et al. Testi. Dust evolution in protoplanetary disks. *Protostars and Planets VI*, 2014.

[57] L. et al. Testi. The protoplanetary disk population in the -ophiuchi region l1688 and the time evolution of class ii ysos. *Astronomy Astrophysics, 663, A98 (2022)*, 2022.

[58] R. Teyssier. Cosmological hydrodynamics with adaptive mesh refinement: a new high resolution code called ramses. *Astronomy Astrophysics, Volume 385, pages 337-364*, 2002.

[59] J. K. et al. Truelove. The jeans condition: A new constraint on spatial resolution in simulations of isothermal self-gravitational hydrodynamics. *Astrophysical Journal, Volume 489, Number 2*, 1997.

[60] Y. et al. Tsukamoto. Effects of ohmic and ambipolar diffusion on formation and evolution of first cores, protostars, and circumstellar discs. *Monthly Notices of the Royal Astronomical Society, Volume 452, Issue 1, 01 September 2015, Pages 278–288*, 2015.

[61] N.. et al. Tung. Accuracy of alma estimates of young disk radii and masses. *Astronomy Astrophysics, 684, A36 (2024)*, 2024.

[62] M. L. R. van 't Hoff and J. B. Bergner. Protoplanetary disk chemistry and structure. *Encyclopedia of Astrophysics*, 2024.

[63] R. W. et al. Wilson. Carbon monoxide in the orion nebula. *Astrophysical Journal, vol. 161, p.L43*, 1970.

[64] A. J. et al. Winter. Protoplanetary disc truncation mechanisms in stellar clusters: comparing external photoevaporation and tidal encounters. *onthly Notices of the Royal Astronomical Society, Volume 478, Issue 2, August 2018, Pages 2700–2722*, 2018.